J. Fluid Mech. (2004), *vol.* 512, *pp.* 95–131.
DOI: 10.1017/S0022112004009814 Printed in the United Kingdom

Sliding, slipping and rolling: the sedimentation of a viscous drop down a gently inclined plane

By S. R. HODGES[1], O. E. JENSEN[2] AND J. M. RALLISON[1]

[1]Department of Applied Mathematics and Theoretical Physics, Centre for Mathematical Sciences, University of Cambridge, Wilberforce Road, Cambridge CB3 0WA, UK

[2]Division of Applied Mathematics, School of Mathematical Sciences, University of Nottingham, University Park, Nottingham NG7 2RD, UK

(Received 25 July 2003 and in revised form 9 April 2004)

We consider the steady sedimentation under gravity of a viscous drop, suspended in a viscous liquid, along a plane tilted at a small angle α to the horizontal. The drop does not wet the wall but is supported by a thin lubricating film of liquid. In the Stokes-flow limit, the problem is parameterized by α, the ratio B of buoyancy to capillary forces (a Bond number) and a viscosity ratio λ. Provided B is not too large ($B \ll \alpha^{-1}$ in two dimensions, $B \ll \alpha^{-4/3}$ in three dimensions), the drop's motion can be described asymptotically by combining a capillary-statics approximation for the drop shape away from the wall, lubrication theory for the thin film and a combination of lubrication theory and a half-plane boundary-integral method for the drop interior.

Systematic scaling arguments for both two- and three-dimensional drops, supported by detailed calculations, are used to survey (B, λ)-parameter space for fixed $\alpha \ll 1$. We find a strong coupling between drop shape (ranging from nearly round to a flattened pancake), kinematics (including slipping, sliding, rolling and tank-treading motions) and the site of dominant viscous dissipation (the edges of the thin film, the bulk of the thin film or the drop interior). Predictions of drop speed and shape are compared with available experimental and computational data.

1. Introduction

In this paper we consider the motion of a viscous drop, of viscosity $\lambda\mu$ and density $\rho + \Delta\rho$, suspended in an external fluid of viscosity μ and density ρ. With $\Delta\rho > 0$, the drop sediments in a vertical gravitational field g toward a plane tilted at an angle $\alpha \ll 1$ to the horizontal; equivalently for $\Delta\rho < 0$ we can consider it rising against the underside of the plane. We assume that the suspending fluid wets the plane so that, after some time, the drop moves steadily along the plane with speed $U^\star$, supported by a lubricating layer of liquid. The component of gravity acting normal to the plane distorts the drop from its initially spherical shape; the degree of distortion is controlled by the Bond number $B = \Delta\rho g a^2/\gamma$, where a is the radius of the undistorted drop and γ is its uniform surface tension. If the drop is very viscous ($\lambda \to \infty$), we expect the distorted drop to slide down the plane without rotating; if the drop is relatively inviscid ($\lambda \to 0$), it will 'slip' down the plane with external viscous stresses driving a passive recirculating flow within the drop. For intermediate viscosity ratios, we expect the drop to move with a combination of sliding, slipping and rolling motions with the internal flow in the drop potentially taking a dominant role in

determining the overall motion. We aim to predict the drop's shape and kinematics when inertial forces are negligible and when the surface tension γ dominates viscous forces everywhere except in the lubricating film beneath the drop. As well as having intrinsic interest in fluid-mechanical terms, this problem has applications to diverse technological processes (such as microfluidics) and to biology (e.g. as a model of an embolism or an adherent cell in a blood vessel).

While numerous authors have examined the effects of walls on the motion of deformable drops and bubbles (for a recent review see Magnaudet, Takagi & Legendre 2003), literature treating the zero-Reynolds-number motion of a non-wetting drop or bubble in close proximity to a nearly horizontal plane is relatively scarce. Masliyah, Jauhari & Gray (1994) performed experiments on bubbles rising under inclined plates at low Reynolds numbers and showed that $U^\star$ increases monotonically with α. Tsao & Koch (1997) measured the speed at which a nearly circular bubble rises beneath a tilted wall. Although their experiments were conducted at moderate Reynolds numbers, they recognized that viscous lubrication forces beneath the deformed bubble could be large enough to balance the gravitational force normal to the plane. Aussillous & Quéré (2002) investigated bubbles rising steadily under a nearly horizontal surface. For large pancake-shaped bubbles (for which a greatly exceeds the capillary length $\sqrt{\gamma/\Delta\rho g}$, so that $B \gg 1$), they used scaling arguments to predict that $U^\star$ is proportional to $a^{9/4}\alpha^{3/2}$ (balancing dissipation in the nose and tail regions of the thin lubricating film with the rate of change of potential energy), and provided experimental data confirming this prediction. For small nearly spherical bubbles (for which $B \ll 1$), they proposed a scaling argument involving the Stokes drag on the bubble; we reconsider this regime below.

The motion of viscous drops is enriched by competition between flows inside and outside the drop. Mahadevan & Pomeau (1999) used scaling arguments to identify an unexpected feature of the motion of non-wetting drops. A small drop (with $B \ll 1$) is almost spherical except for a flat spot at its base. They predicted that such a drop rolls down a gently tilted plane in solid-body rotation throughout its interior except for a small region above the flat spot. Balancing viscous dissipation in this small region with the rate of change of potential energy of the drop, they found that U is proportional to $1/a$ (i.e. small drops roll quicker than large ones). They also predicted that pancake-shaped drops (with $B \gg 1$) roll down a surface at a speed independent of $\Delta\rho g$. These predictions were confirmed experimentally by Richard & Quéré (1999) (using small liquid drops rolling down highly hydrophobic surfaces) and Aussillous & Quéré (2001) (using small droplets coated with a hydrophobic powder to make them non-wetting 'liquid marbles'). Abkarian, Lartigue & Viallat (2001) showed how phospholipid vesicles of dimensions 10–50 μm, suspended in liquid, move by a combination of sliding and rolling under gravity along a plane surface. This motion was modelled using the classical theory of Goldman, Cox & Brenner (1967) for a sphere moving near a wall, assuming a minimum separation distance of around 0.05 μm, a distance at which thermodynamic fluctuations of the vesicle's membrane may be significant.

DeBisschop, Miksis & Eckmann (2002) used a boundary-integral method to compute the unsteady motion of a train of two-dimensional drops in an inclined channel, allowing for the presence of surfactants but assuming the viscosity ratio $\lambda = 1$. They showed how, under certain circumstances, drops can assume a steady configuration (although the time taken for transients to decay increases as the channel became more horizontal) and they computed the dependence of bubble speed and shape on parameters including B and α.

The literature treating the motion of a non-wetting drop near a gently inclined plane is therefore patchy: a number of intriguing phenomena have been identified, and isolated regions in parameter space have been studied, but no systematic survey of parameter space is yet available. To remedy this, we use scaling arguments to map out regions in (B, λ)-parameter space (for fixed $\alpha \ll 1$) for both two- and three-dimensional drops characterizing asymptotically distinct changes in drop shape, sites of dominant viscous energy dissipation and drop kinematics (see figures 4 and 12 below). We then use asymptotic approximations (capillary statics for the drop shape away from the wall, lubrication theory for the thin gap and, where necessary, a half-plane two-dimensional boundary-integral method (Hodges, Jensen & Rallison 2004) or lubrication theory for the internal flow) to determine the coefficients in front of the terms identified by scaling arguments.

The organization of the paper is as follows. We treat two-dimensional drops in some detail (§§2–5), partly to explain scaling arguments carefully (summarized in table 1), partly because of some intrinsic complications of two-dimensional motion and partly because two-dimensional features prove to be an essential ingredient of three-dimensional calculations. In §2 we analyse the static 'sessile' drop shape and describe the physical ingredients of the sedimenting drop problem, defining the terms 'sliding', 'slipping', 'rolling' and 'tank-treading' for possible drop motions. In §3 we use these ingredients to obtain scaling estimates for the drop velocity and layer thickness for the different regions of parameter space that we have identified. In §4, we solve the lubrication equations to find numerical coefficients for our scaling estimates for extreme values of the parameters, and in §5 we give a physical description of our results and compare them with the two-dimensional computations of DeBisschop *et al.* (2002). Three-dimensional drops are given a more succinct treatment in §§6–8: scalings in this case are derived in §6 and are summarized in table 3, numerical coefficients are computed in §7 and predictions are discussed in the light of available experiments in §8.

2. Two-dimensional drops: preliminaries

We begin by setting the stage for a systematic scaling argument presented in §3 below. We first recall briefly the shape of a sessile non-wetting drop resting on a horizontal wall.

2.1. *Sessile two-dimensional drop*

Suppose a two-dimensional drop rests statically on a horizontal wall, as shown in figure 1(*a*). Scaling lengths on the drop's undistorted radius a and pressures on the capillary scale γ/a, the shape of the free boundary $Z = H(X)$ (measuring X along and Z normal to the wall) is determined by the Young–Laplace equation $P_d - BH = \kappa$, where the constant P_d is the static internal pressure, B the Bond number and $\kappa = \pm H_{XX}/(1 + H_X^2)^{3/2}$ the curvature, with the sign determined by whether one considers the upper $(-)$ or lower $(+)$ branch of the curve. The base of the drop makes contact with the wall, and we take the contact angle to be zero, so that $H_X = 0$ where $H = 0$; we also impose the symmetry condition $H_X(0) = 0$. To determine P_d, we impose the constraint that the drop has fixed area π; P_d is also the drop curvature at the wall where $H = 0$. The Young–Laplace equation may be integrated once to give $P_d H - \frac{1}{2}BH^2 = 1 \mp (1 + H_X^2)^{-1/2}$. If H_d is the maximum height of the drop then

$$P_d = (2/H_d) + \tfrac{1}{2}BH_d. \tag{2.1}$$

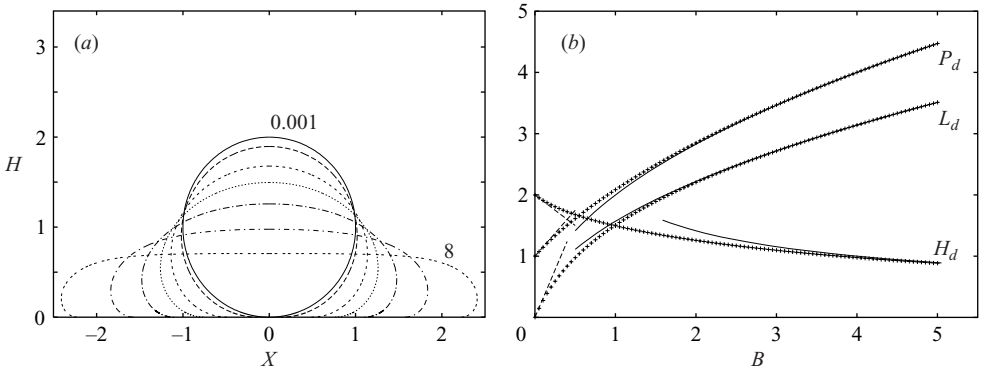

FIGURE 1. (*a*) Shapes of a static sessile drop for $B = 0.001$, 0.1, 0.5, 1, 2, 4, 8. (*b*) The internal drop pressure P_d, the contact length between drop and wall L_d, and the maximum drop height H_d are plotted versus B. Solid lines show asymptotes (2.3) for $B \gg 1$; dashed lines show asymptotes for $B \ll 1$.

The weight of the drop, πB, is supported by hydrostatic stresses along its flat base. There is no contribution to the vertical force balance arising from surface tension because the contact angle is zero. If the length of contact between the drop base and the wall is L_d, then

$$P_d L_d = \pi B. \tag{2.2}$$

A unique shape may be computed for each value of B, as shown in figure 1. (In order to avoid using the multi-valued function $H(X)$ it is computationally convenient to represent the drop in intrinsic coordinates, see O'Brien 1991). For $B \gg 1$, gravity dominates surface tension and the drop is flattened against the wall. In this limit κ is small when $H = H_d$ and therefore $P_d \approx B H_d$, so that

$$P_d \approx 2B^{1/2}, \quad L_d \approx \tfrac{1}{2}\pi B^{1/2}, \quad H_d \approx 2B^{-1/2} \tag{2.3}$$

(as shown in figure 1*b*). For $B \ll 1$ the drop is near-circular, and $P_d \approx 1 + \frac{3}{2}B$, $L_d \approx \pi B - \frac{3}{2}\pi B^2$ and $H_d \approx 2 - B$. Notice that, for all Bond numbers, $P_d \sim H_d^{-1}$ (where $\sim$ denotes 'scales like'). Although our analysis is valid when B is of order unity, we do not have closed-form expressions for P_d, L_d and H_d in this case; computed values are shown in figure 1(*b*).

2.2. *A sedimenting drop at low capillary number*

Suppose now that the drop sediments steadily down a plane wall inclined at an angle α to the horizontal. Gravity causes the drop to move relative to the wall with centre of mass speed $U^\star = \gamma U/\mu$ to be determined, where μ is the viscosity of the suspending fluid. The non-dimensional velocity U has the significance of a capillary number.

Because $U = 0$ when $\alpha = 0$, we may consider the parameter regime $\alpha \ll 1$ in which U remains small and the fluid stresses on the outer part of the drop are weak. If, in addition, pressures associated with the internal flow are small compared with P_d, then the static balance is maintained. The drop shape is thus as described in § 2.1, except that the flat spot that was in contact with the wall becomes the lower drop boundary. In general we anticipate that the drop rests on a lubricating film of thickness $\epsilon \ll 1$ to be determined (figure 2). The thickness of this film controls the rate at which external fluid can enter the gap between the wall and the drop and therefore is related to U.

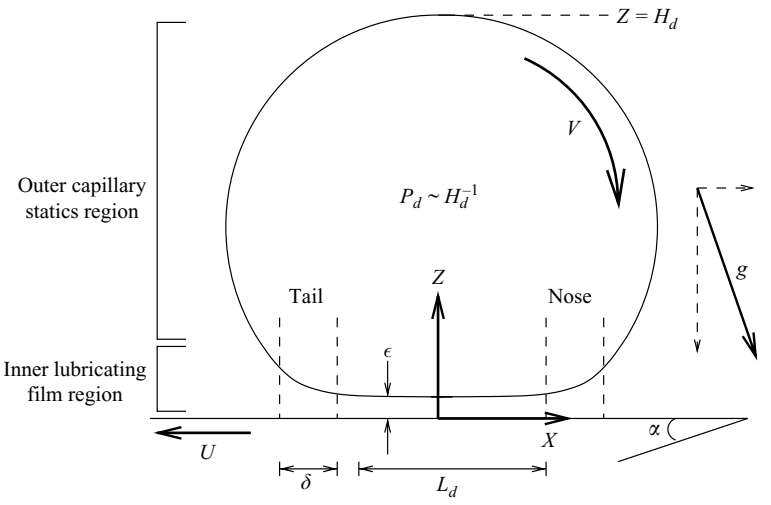

FIGURE 2. Sketch of a drop sedimenting down an inclined wall in a frame of reference fixed to the moving drop, showing 'outer' and 'inner' regions and lengths H_d, L_d, ϵ and δ.

In general, the drop moves by a combination of sliding, slipping, rolling or tank-treading (the precise meanings of these terms in the present context are defined in § 2.6 below) so that a typical dimensionless internal fluid velocity is V. The dynamic problem is controlled by three independent dimensionless parameters: the Bond number B; the wall tilt angle α; and the ratio of internal to external viscosity λ. Our aim in this and the following section is to obtain scaling estimates for U, V, ϵ and the steady drop shape in terms of B, α, and λ. The drop size appears only within the parameter B; the drop viscosity appears only within the parameter λ.

The external flow around the main body of the drop creates stresses of magnitude U/H_d (relative to a dimensional stress scale γ/a). Viscous stresses in the drop are no larger than $\lambda V/H_d$. Thus viscous stresses are small compared to the static internal pressure $P_d \sim H_d^{-1}$ provided that $U \ll 1$ and $\lambda V \ll 1$. For long thin drops ($B \gg 1$) a stronger condition for the neglect of internal pressure variations is needed, because a pressure difference $\lambda V L_d H_d^{-2}$ is required between the front and rear to maintain zero net flux. This pressure is small compared to P_d (see (2.3)) only if $\lambda V B \ll 1$. Therefore the internal and external flows are sufficiently weak to preserve the sessile shape provided the capillary numbers λV, $\lambda B V$ and U are all much less than unity. We shall find later, once U and V have been calculated, that for all values of λ these conditions are satisfied provided $B \ll \alpha^{-1}$.

2.3. *Governing equations*

We choose a frame of reference fixed relative to the drop and (X, Z)-axes parallel and perpendicular to the wall, as shown in figure 2. The Stokes equations inside the drop are given in dimensionless form (using a modified pressure that absorbs the hydrostatic pressure gradient in the external fluid) as

$$\nabla \cdot \boldsymbol{u} = 0, \qquad \boldsymbol{0} = -\nabla p + \lambda \nabla^2 \boldsymbol{u} + B(\sin\alpha\, \boldsymbol{e}_X - \cos\alpha\, \boldsymbol{e}_Z) \tag{2.4}$$

and for the external fluid

$$\nabla \cdot \boldsymbol{u} = 0, \qquad \boldsymbol{0} = -\nabla p + \nabla^2 \boldsymbol{u}. \tag{2.5}$$

In addition, we have continuity of $\boldsymbol{u}$ across the drop boundary, and $\boldsymbol{u} = (-U, 0)$ on $Z = 0$ and as $|\boldsymbol{X}| \to \infty$. The discontinuity of traction $\boldsymbol{\sigma} \cdot \boldsymbol{n}$ across the drop interface $Z = H(X)$, where $\boldsymbol{n}$ is the unit outward normal to the drop, can be written for small α as

$$[\boldsymbol{\sigma} \cdot \boldsymbol{n}] = \kappa \boldsymbol{n} + B(X\alpha - H)\boldsymbol{n}. \tag{2.6}$$

Integrating over the drop surface S gives the overall force and torque balances

$$\int_S \boldsymbol{\sigma} \cdot \boldsymbol{n} \, \mathrm{d}S = \pi B \alpha \boldsymbol{e}_X - \pi B \boldsymbol{e}_Z, \quad \int_S \boldsymbol{X} \wedge (\boldsymbol{\sigma} \cdot \boldsymbol{n}) \, \mathrm{d}S = \boldsymbol{0}. \tag{2.7a,b}$$

The gravity term on the right-hand side of (2.6) is $-BH$ to leading order, as for a sessile drop; however for $B \gg 1$, X scales as $B^{1/2}$ and H as $B^{-1/2}$ (see (2.3)), so that when $B \sim \alpha^{-1}$ the static balance no longer applies. We consider only the regime $B \ll \alpha^{-1}$.

For the 'inner' film region below the drop (figure 2) we write $Z = \epsilon z$ and $H = \epsilon h$. In $0 \leqslant z \leqslant h(X)$ the Stokes equations (2.5) reduce to those of lubrication theory ($0 = -p_X + u_{ZZ}$, $0 = -p_Z$) with $u = -U$ at $z = 0$ and

$$u_z|_{z=h^-} = \lambda u_z|_{z=h^+}, \qquad u|_{z=h^-} = u|_{z=h^+}. \tag{2.8a,b}$$

2.4. *Length and velocity scales*

The drop sketched in figure 2, which is representative of many but not all drop shapes that we consider, has five asymptotic regions: the film below the flat spot which has the form of a straight-sided channel; the film's nose and tail where the interfacial curvature varies rapidly; the flow within the drop; and the external flow over the main body of the drop. There are four lengthscales, all in general different: (i) the length L_d of the flat spot; (ii) the drop height H_d; (iii) the thickness ϵ of the film; and (iv) the lengthscale δ of the nose and tail.

Provided the drop has a distinct flat spot, the flux in the film is controlled by the nose region (Landau & Levich 1942; Bretherton 1961) where the drop curvature changes by H_d^{-1}. Because the leading-order curvature of the boundary is H_{XX}, the lengths of the nose and tail must scale as $\delta \sim (\epsilon H_d)^{1/2}$. Pressure variations p in the external fluid arising from surface tension in the nose and tail regions have magnitude H_d^{-1}. The corresponding pressure gradients drive a steady flux that scales as $Q \sim H^3 p_X \sim (\epsilon^5 / H_d^3)^{1/2}$, so that the sliding speed scales as

$$U \sim (\epsilon / H_d)^{3/2}. \tag{2.9}$$

These scaling estimates cease to be appropriate if the distinct flat spot disappears. We show later that this occurs only for $B \lesssim \alpha$.

2.5. *Force and energy balances*

As indicated in figure 1(*a*), for large B a sessile drop has a pancake shape; for small B it has a small but distinct flat spot at its base. If, when the drop moves, the nose and tail regions shown in figure 2 merge, we can identify a third possibility, arising for very small B, namely a circular drop with no identifiable flat spot. These three possibilities are sketched in figure 3 and are denoted P, F and C respectively.

There are two candidates for the force required to support the weight normal to the wall, πB. One is the pressure P_d below the flat spot. In that case, the normal force balance is simply the static balance (2.2). A second possibility is the dynamic pressure arising from motion in the film. We will show that this is the case when $B \lesssim \alpha$ and the nose and tail overlap (case C, figure 3). The two effects are comparable when $B \sim \alpha$.

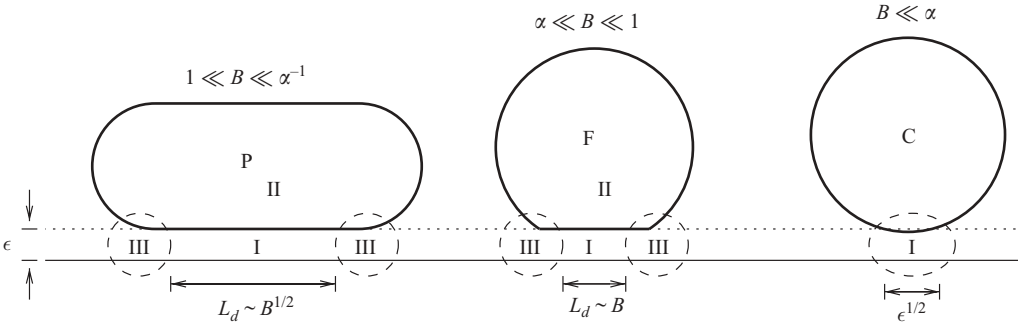

FIGURE 3. Sketch of the P (pancake), F (flat spot), and C (circular) drop shapes. The notation I, II, III indicates areas of principal energy dissipation.

There are also two candidates for balancing the weight tangential to the wall, $\pi B\alpha$ (see (2.7*a*)). For large λ, shear stresses in the film support the weight. For small λ, the weight is balanced by a net pressure force resulting from the difference in shape between the nose and tail. We will show that the viscous drag on the outer drop surface is negligible provided $B \ll \alpha^{-1}$.

As the drop moves, gravitational potential energy is dissipated at rate $UB\alpha$ in one or more of three regions shown in figure 3: region I is the film; region II is the drop interior; and region III is the film nose and tail. The scaling argument in § 3 below shows how dissipation in each region (I, II, III) dominates in some part of (B, λ)-parameter space. To aid the discussion to follow, a summary for fixed $\alpha \ll 1$ is sketched in figure 4 with the corresponding scalings given in table 1. All of the scalings are justified in detail in later sections. Each region in the diagram is labelled by both a letter corresponding to the drop shape: P (a pancake, $1 \ll B \ll \alpha^{-1}$); F (near-circular, but with a flat-spot, $\alpha \ll B \ll 1$); or C (near-circular with no flat-spot, $B \ll \alpha \ll 1$) and also with I, II or III corresponding to the principal region of dissipation. For a near-circular drop (case C), there is a single scaling for U and ϵ; the subscripts 1, 2, 3, 4 in table 1 correspond to different scalings for the internal drop speed V.

2.6. *Drop kinematics: sliding, slipping and rolling*

In all circumstances the internal fluid velocity V cannot exceed U. For $\lambda \to \infty$, no internal motion is possible and the drop moves as a solid body. Because the drop is never perfectly circular, the only possible motion has $V = 0$; we term this motion *sliding*. In that case the boundary condition (2.8*b*) reduces at leading order to $u = 0$ on $z = h(X)-$. As λ is reduced, internal motion becomes possible. We identify the lower limit for sliding as the smallest magnitude of λ for which $u = 0$ can be applied in a leading-order asymptotic approximation. In figure 4, regions $\mathrm{CI}_{1,2,3}$, FI and PI all meet this defintion of sliding.

At the opposite extreme, if $\lambda = 0$ the internal flow generates no stress and therefore has no dynamic effect on the film. In this case V is comparable with U and the boundary condition (2.8*a*) becomes (at leading order) $u_z = 0$ on $z = h(X)-$. We term a motion *slipping* if this zero shear stress condition can be applied. In figure 4, regions CI_4, FIII_2, PIII and PII_2 correspond to slipping.

As λ is increased from zero, the slipping condition first fails in the nose and tail regions where velocity variations of magnitude U over a length δ generate stresses within the drop of magnitude $\lambda U/\delta$. Slipping occurs only when these stresses are

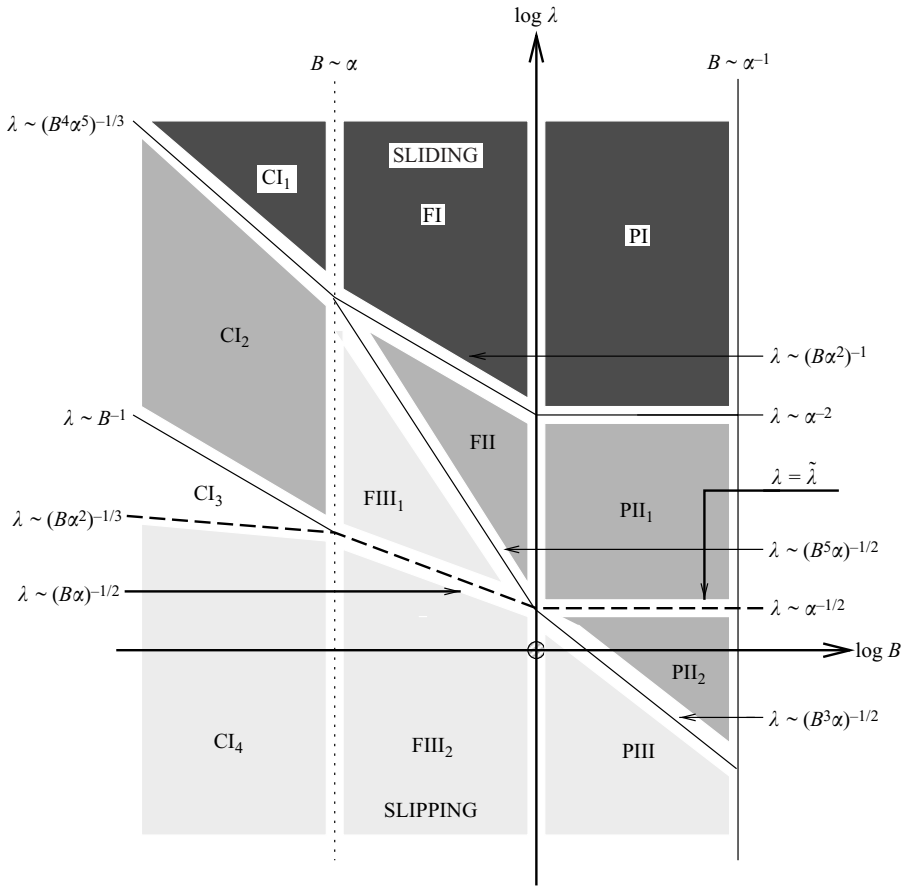

FIGURE 4. Sketch of (B, λ)-parameter space with $\alpha \ll 1$. In regions C the drop is near-circular without a flat spot; in regions F it has a flat spot on its base; in regions P the drop is pancake-shaped. The principal location for energy dissipation is the film for regions labelled I; internally for regions labelled II; and in the nose and tail of the film for regions labelled III. Solid lines delimit different asymptotic behaviours; the dashed line defines the upper limit of slipping where the interface rigidity $\tilde{\lambda} = O(1)$.

small compared with the shear stress in the film, U/ϵ. Thus the upper asymptotic limit for slipping is given by $\lambda = \delta/\epsilon \sim (H_d/\epsilon)^{1/2}$. The group $\tilde{\lambda} = \lambda(\epsilon/H_d)^{1/2}$ is the 'interface rigidity' (Davis, Schonberg & Rallison 1989) for the nose and tail; if it is small the boundary remains mobile and stress-free, but if large, velocity variations are suppressed and the interface moves with a uniform velocity. Perhaps surprisingly, the interface rigidity plays only a minor role in this problem. When $\tilde{\lambda} = O(1)$, the internal flow affects the nose and therefore modifies the thickness of the film and the drop speed, but only by a numerical factor (Hodges *et al.* 2004). More important is that for intermediate λ (sometimes larger and sometimes smaller than $\tilde{\lambda}$) an internal flow throughout the drop is established with $V \sim U$. Such a flow can and does affect the scalings of the force balance and drop speed. The internal motion takes the form of *tank-treading*, where the internal velocity V is uniform over the flat spot if the drop is pancake-shaped (figure 5*b*), or *rolling*, consisting of a solid-body rotation with angular velocity V, together with an asymptotically smaller perturbation flow, if the drop is near-circular (case C, figure 3 or F, figure 5*a*).

Region	Motion	ϵ	L_d	δ	U	V	p
PI	Sliding	$B^{-1/2}\alpha^2$	$B^{1/2}$	$B^{-1/2}\alpha$	α^3	α/λ	$B^{1/2}$
PII_1	Tank	$B^{-1/2}(\alpha/\lambda)^{2/3}$	$B^{1/2}$	$B^{-1/2}(\alpha/\lambda)^{1/3}$	α/λ	α/λ	$B^{1/2}$
PII_2	Slipping	$B^{-1/2}(\alpha/\lambda)^{2/3}$	$B^{1/2}$	$B^{-1/2}(\alpha/\lambda)^{1/3}$	α/λ	α/λ	$B^{1/2}$
PIII	Slipping	$B^{1/2}\alpha$	$B^{1/2}$	$\alpha^{1/2}$	$(B\alpha)^{3/2}$	$(B\alpha)^{3/2}$	$B^{1/2}$
FI	Sliding	α^2	B	α	α^3	$\alpha/B\lambda$	1
FII	Rolling	$(\alpha/B\lambda)^{2/3}$	B	$(\alpha/B\lambda)^{1/3}$	$\alpha/B\lambda$	$\alpha/B\lambda$	1
$FIII_1$	Rolling	$B\alpha$	B	$(B\alpha)^{1/2}$	$(B\alpha)^{3/2}$	$(B\alpha)^{3/2}$	1
$FIII_2$	Slipping	$B\alpha$	B	$(B\alpha)^{1/2}$	$(B\alpha)^{3/2}$	$(B\alpha)^{3/2}$	1
CI_1	Sliding	$(B\alpha^2)^{2/3}$	0	$(B\alpha^2)^{1/3}$	$(B^4\alpha^5)^{1/3}$	$(B/\alpha)^{2/3}/\lambda$	$(B/\alpha)^{1/3}$
CI_2	Slide/Roll	$(B\alpha^2)^{2/3}$	0	$(B\alpha^2)^{1/3}$	$(B^4\alpha^5)^{1/3}$	$B^2\alpha$	$(B/\alpha)^{1/3}$
CI_3	Sliding	$(B\alpha^2)^{2/3}$	0	$(B\alpha^2)^{1/3}$	$(B^4\alpha^5)^{1/3}$	$B\alpha/\lambda$	$(B/\alpha)^{1/3}$
CI_4	Slipping	$(B\alpha^2)^{2/3}$	0	$(B\alpha^2)^{1/3}$	$(B^4\alpha^5)^{1/3}$	$(B^4\alpha^5)^{1/3}$	$(B/\alpha)^{1/3}$

TABLE 1. Scalings for film thickness, ϵ, length of the flat spot, L_d, length of the nose and tail regions, δ, drop speed, U, internal fluid velocity, V, and pressure below the drop, p. Lengths are scaled on a, velocities on γ/μ and pressures on γ/a. Region CI_2 is labelled both sliding and rolling because the drop rolls with $V \ll U$.

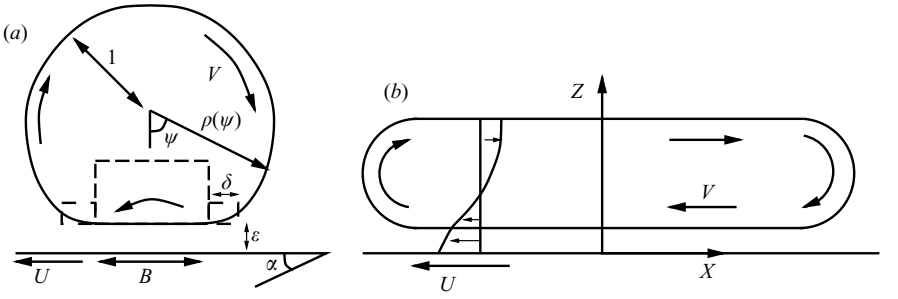

FIGURE 5. Sketch showing the internal flow for (*a*) rolling (case F) and (*b*) tank-treading (case P).

As noted in table 1, there are circumstances (case CI_2) where a near-circular drop rolls with angular velocity much smaller than U, so that it also meets the definition of sliding; rolling and sliding are not mutually exclusive.

3. Two-dimensional drops: scalings

We now provide detailed justification for the scalings summarized in table 1 and figure 4. The scalings here underpin the formal derivations of numerical coefficients in § 4 below.

3.1. *Near-circular drop with a flat spot: cases FI, FII, FIII:* $\alpha \ll B \ll 1$

For $\alpha \ll B \ll 1$, the drop is almost circular, with a flat spot of length B. The nose and tail have lengths $\delta \sim \epsilon^{1/2}$ that are small compared with the flat spot. The internal motion is solid-body rotation with angular velocity V, but the $O(B)$ deformation of the circular shape gives rise to perturbation velocities of magnitude BV in the main body of the drop to meet $\boldsymbol{u}\cdot\boldsymbol{n} = 0$ on the drop boundary. This perturbation flow generates internal stresses of magnitude λBV in the main body of the drop,

larger stresses of magnitude λV in a region of size B above the flat spot, and even larger stresses $\lambda V B/\delta$ above the nose and tail (figure 5*a*). The rate of viscous energy dissipation in each of these three regions is $\lambda B^2 V^2$.

3.1.1. *Region FI:* $\lambda \gg (B\alpha^2)^{-1}$

A very viscous drop ($\lambda \to \infty$) slides with negligible internal motion. Its weight normal to the wall, πB, is supported by the pressure P_d in the film. The Couette flow in the film gives stresses of size U/ϵ over the flat spot of length B that support the down-slope weight, $\pi B\alpha$. From (2.9), $U \sim \epsilon^{3/2}$ so $U \sim \alpha^3$ and $\epsilon \sim \alpha^2$. The sliding speed and film thickness are thus independent of both the internal viscosity and the Bond number.

Shear stresses over the flat spot create a torque of magnitude $B\alpha$ about the drop centre. This torque is balanced by a higher-order perturbation pressure in the film of magnitude $\alpha/B \ll 1$ associated with a perturbation velocity having magnitude $\alpha^5/B^2 \ll U$.

The fluid inside the drop is subjected to tangential tractions of magnitude α and larger normal tractions of magnitude α/B, giving an internal flow of magnitude $V \sim \alpha/B\lambda$. Viscous dissipation is largest in the film, so that the leading-order energy balance is $UB\alpha \sim (U/\epsilon)^2 \epsilon B$. Internal dissipation scales as $\lambda V^2 B^2 \sim \alpha^2/\lambda$ and is comparable with that in the film when $\lambda \sim (B\alpha^2)^{-1}$. At the same value of λ, the rolling speed V becomes comparable with the sliding speed U, reducing the shear traction in the film. Thus the lower boundary of region FI is at $\lambda \sim (B\alpha^2)^{-1}$, as shown in figure 4.

3.1.2. *Region FII:* $(B^5\alpha)^{-1/2} \ll \lambda \ll (B\alpha^2)^{-1}$

If $\lambda \ll (B\alpha^2)^{-1}$, energy is lost predominantly in the drop interior, the speeds U and V are comparable, and the energy balance $UB\alpha \sim \lambda V^2 B^2$ yields $V \sim U \sim \alpha/(B\lambda)$. It follows from (2.9) that $\epsilon \sim (\alpha/B\lambda)^{2/3}$. This result is the two-dimensional equivalent of Mahadevan & Pomeau's (1999) scalings for a three-dimensional rolling drop that wets an inclined wall: the velocity of the rolling drop is independent of the viscosity of the outer fluid and, remarkably, the drop moves down the wall at a speed inversely proportional to the gravitational acceleration g. The reason is that although the gravitational driving force increases with B (scaling as B), the internal viscous dissipation increases even faster (scaling as B^2).

3.1.3. *Region FIII:* $\lambda \ll (B^5\alpha)^{-1/2}$

If the drop is inviscid ($\lambda = 0$) it slips and the flow profile in the film is uniform. Shear stresses in the film cannot support the down-slope weight, but the different pressure distributions corresponding to the different shapes of the nose and tail provide the tangential force. The pressure in the nose and tail is of order unity, their lengths scale as $\epsilon^{1/2}$, and the down-slope component of the surface normal also scales as $\epsilon^{1/2}$. The force balance is therefore $\epsilon \sim B\alpha$. It follows from (2.9) that U and V scale as $(B\alpha)^{3/2}$. In this case dissipation is greatest in the nose and tail and therefore the energy balance is $UB\alpha \sim (U/\epsilon)^2 \delta\epsilon$. We show in § 4.2.2 below that in these circumstances a drop experiences no net couple: the pressure force on the drop has components both tangential and normal to the wall, and the resulting torques are precisely equal and opposite.

As λ is increased from zero, the interface rigidity $\lambda\epsilon^{1/2}$ of the nose and tail becomes order unity when $\lambda \sim (B\alpha)^{-1/2}$. At this point slipping ceases although the scalings are unaffected. If λ is increased further, internal dissipation $\lambda V^2 B^2$ increases; when

$\lambda \sim (B^5\alpha)^{-1/2}$, internal dissipation dominates and we enter region FII, as shown in figure 4.

3.2. *Pancake drops: cases PI, PII, PIII:* $1 \ll B \ll \alpha^{-1}$

When $B \gg 1$, the drop length $L_d \sim B^{1/2}$ and height $H_d \sim B^{-1/2}$ (see (2.3)). The length of the nose and tail is $\delta \sim \epsilon^{1/2}B^{-1/4}$, and therefore (2.9) implies that $U \sim \epsilon^{3/2}B^{3/4}$. The static description given in § 2.1 breaks down when B becomes as large as α^{-1} for two reasons. First, the fore–aft-symmetric sessile drop shape is no longer the static equilibrium (see (2.7*a*)); this constraint applies for all λ. Second, the internal capillary number λBV (see § 2.2) becomes comparable with unity; this constraint (it turns out) applies in regions PI and PII, but not in PIII.

3.2.1. *Region PI:* $\lambda \gg \alpha^{-2}$

A very viscous pancake-shaped drop slides with negligible internal motion and its weight normal to the wall is supported by the pressure $P_d = O(B^{1/2})$ in the film. The flow in the film gives tangential stresses of size U/ϵ acting over a length $B^{1/2}$ that support the down-slope weight, $\pi B\alpha$. From (2.9) it follows that $U \sim \alpha^3$ and $\epsilon \sim B^{-1/2}\alpha^2$. This scaling for U is the same as that in region FI but the film thickness is a factor $B^{-1/2}$ smaller.

If the condition $\lambda \to \infty$ is relaxed but λ remains large, a slow internal tank-treading V is generated. The internal stress has magnitude $\lambda B^{1/2}V$, so V scales as α/λ. Energy is lost predominantly to dissipation in the film.

When $\lambda \sim \alpha^{-2}$, the velocities U and V become comparable and dissipation in the interior, of magnitude $\lambda V^2 B$, becomes comparable with that in the film. The shear rate in the film $(U - V)\epsilon^{-1}$ is reduced and although shear stresses along the drop base still support the tangential component of the weight, the scalings change. This provides the lower limit on λ for region PI.

3.2.2. *Region PII:* $(B^3\alpha)^{-1/2} \ll \lambda \ll \alpha^{-2}$

If $\lambda \lesssim \alpha^{-2}$, the drop tank-treads and dissipation is largest inside the drop. Shear stresses in the film drive a flow inside the drop with $V \sim U$. The energy balance $UB\alpha \sim \lambda V^2 B$ yields $V \sim U \sim \alpha/\lambda$. From (2.9), the thickness of the film is $\epsilon \sim B^{-1/2}(\alpha/\lambda)^{2/3}$. The velocity of a tank-treading pancake drop is independent of both B and the viscosity of the outer fluid (cf. Mahadevan & Pomeau 1999).

3.2.3. *Region PIII:* $\lambda \ll (B^3\alpha)^{-1/2}$

If the drop is inviscid it slips, the pressure in the nose and tail provides the tangential force $\delta(\epsilon/\delta)B^{1/2} \sim B\alpha$ and so the film has thickness $\epsilon \sim B^{1/2}\alpha$. It follows from (2.9) that U and V scale as $(B\alpha)^{3/2}$. The torques generated by the pressure in the nose and tail balance exactly.

Dissipation is largest in the nose and tail, giving an energy balance $UB\alpha \sim (U/\epsilon)^2\delta\epsilon$. As λ is increased past $(B^3\alpha)^{-1/2}$ internal dissipation dominates and we enter region PII, as shown in figure 4. Surprisingly, the region where the slip boundary condition is appropriate overlaps PII because the interface rigidity of the nose and tail does not become of order unity until $\lambda \sim \alpha^{-1/2}$. The thickness of the film in PII_2 therefore has the same magnitude as that associated with an inviscid bubble. In region PII_2 the leading-order velocity profile in the film is uniform, but an additional weak shear provides the force which supports the down-slope weight.

3.3. *Near-circular drop: cases CI_1–CI_4: $B \ll \alpha$*

When B becomes as small as α, the lengths of the nose, tail and flat spot are all comparable. In cases CI_1–CI_4, for which $B \ll \alpha$, the drop boundary is near-circular with a single region of deformation with length $O(\epsilon^{1/2})$. In consequence, the flat-spot description of the shape is no longer appropriate, the velocity scaling (2.9) is no longer valid, and the weight can no longer be supported by the surface-tension-generated film pressure.

Because the drop is near-circular, we express its radius as $\rho(\psi) = 1 + df(\psi)$, where $d \ll 1$ is to be determined and ρ and ψ are as defined in figure 5(a). We suppose that the function $f(\psi)$ is of order unity and $f \to 0$ as $|\psi|$ becomes larger than $O(\epsilon^{1/2})$. As the drop moves, there is high pressure in the film in front of the drop and low pressure behind. To maintain a steady flux in the film, this pressure difference must scale as $p_1 \sim U\epsilon^{-3/2}$, contributing a net tangential force of size $U\epsilon^{-1/2}$ that supports the down-slope weight $B\alpha$. Therefore $U \sim B\alpha\epsilon^{1/2}$ and $p_1 \sim B\alpha\epsilon^{-1}$. The net tangential force due to shear on the drop base cannot exceed $U\epsilon^{-1/2}$ and this is comparable with, or smaller than, the pressure force. Thus the estimate is unaffected by the inclusion of shear and the scaling of U is independent of λ.

The curvature of the boundary is $\kappa = 1 - d(f + f_{\psi\psi}) + O(d^2)$. This changes by an amount d/ϵ over the film, so $p_1 \sim d/\epsilon$. Comparing with the estimate above, we have $d \sim B\alpha$.

It might be thought that p_1 also supplies the force which supports the weight normal to the wall. This is not the case because the leading-order pressure is fore–aft anti-symmetric. Instead, p_1 deforms the drop shape against surface tension so that the upstream side is pushed further from the wall than the downstream side. This deformation generates a perturbation pressure in the film p_2 that supplies the normal force, as in a slider bearing. The difference in surface displacement between the front and rear has magnitude d. So the relative change in film thickness (the perturbation divided by the original thickness) has size d/ϵ. The corresponding additional pressure p_2 is fore–aft symmetric and has magnitude $p_2 \sim (d/\epsilon)p_1 \sim (d/\epsilon)^2$, giving rise to a normal force of size $(B\alpha)^2\epsilon^{-3/2}$ that balances the weight πB. It follows that $\epsilon \sim (B\alpha^2)^{2/3}$, $U \sim (B^4\alpha^5)^{1/3}$, as given in table 1 and, correspondingly, $p_1 \sim d/\epsilon \sim (B/\alpha)^{1/3}$ and $p_2 \sim (B/\alpha)^{2/3}$.

It remains to determine the magnitude V of the flow inside the drop. In two dimensions this proves to depend on λ in a surprisingly complicated way; the corresponding result for a near-sphere is comparatively simple (see § 7.2.1 below).

A near-circular drop rolls with angular velocity V. Perturbations to this motion arise for three reasons. First, the $O(B)$ distortion from a perfect circle gives rise to a perturbation flow of magnitude BV everywhere inside the drop. Second, and more important, there is a perturbation flow with magnitude larger than BV (but smaller than V), caused by the deformation of the base. Because the normal is $\boldsymbol{n} = \boldsymbol{e}_r - df_\psi \boldsymbol{e}_\psi$, this velocity has magnitude $Vd\epsilon^{-1/2}$ in order to meet the condition $\boldsymbol{u}\cdot\boldsymbol{n} = 0$, giving rise to internal normal stresses of magnitude $\lambda V\, d\,\epsilon^{-1} \sim \lambda V(B/\alpha)^{1/3}$ near the base. Third, shear stresses are imposed by the film on the base. The internal velocity varies on a length-scale $\epsilon^{1/2}$, so $(U - V)/\epsilon \sim \lambda V/\epsilon^{1/2}$. Thus, the internal shear-driven velocity V has magnitude $U/\lambda\epsilon^{1/2}$, or U if this is smaller, with a transition between these two behaviours where the interface rigidity is of order unity, i.e. when $\lambda \sim \epsilon^{-1/2} \sim (B\alpha^2)^{-1/3}$.

The scaling for V depends upon whether it is the drop rolling velocity or the internal shear-driven flow that is larger.

In the solid-body limit, the shear-driven flow is negligible and the rolling speed may be estimated by a couple balance. For a rigid circular cylinder that rotates with angular velocity V at a distance $\epsilon \ll 1$ from a stationary wall, the couple on the cylinder scales as $V/\epsilon^{1/2}$. Remarkably, if the rigid cylinder translates relative to a wall with velocity U but does not rotate, then it experiences no net couple (Jeffrey & Onishi 1981); it is this feature that makes the two-dimensional problem special. The drop is a rigid circular cylinder at leading order, so the leading-order flow having pressure p_1 generates no net couple. Furthermore, symmetry implies that the perturbation flow with pressure p_2 also exerts no net couple and nor does the cross-term that arises from p_1 and the leading-order shape change. Therefore it is perturbations of size $p_2 d/\epsilon \sim B/\alpha$ that provide the leading-order couple on the drop, having magnitude $(B/\alpha)\epsilon^{1/2}\epsilon^{1/2} \sim B^{5/3}\alpha^{1/3}$. There are also third-order pressure corrections $p_3 \sim B/\alpha$, but these exert no couple about the drop centre because the leading-order shape is circular. If internal stresses are negligible, this torque causes the drop to rotate with small angular velocity $V \sim \epsilon^{1/2} B^{5/3}\alpha^{1/3} \sim B^2\alpha \ll U$.

There are two reasons for modifying this estimate. If λ is large but not infinite, internal stresses become important, while if λ is small, the internal shear-driven flow becomes larger. We consider these possibilities in turn.

For $\lambda \to \infty$ the drop slides. The magnitude of the internal normal stress at the drop boundary is $\lambda V(B/\alpha)^{1/3}$, and this contributes to the couple balance and inhibits rolling when it is comparable with the normal stress p_3 in the film, i.e. when $V \sim (B/\alpha)^{2/3}/\lambda$. As λ is reduced, V increases from zero until $V \sim B^2\alpha$. At this point we enter the slow-rolling region discussed above. The transition takes place at $\lambda \sim (B^4\alpha^5)^{-1/3}$ and provides the boundary between regions CI_1 (sliding) and CI_2 (sliding with slow rolling) as shown in figure 4. For yet smaller λ, the internal shear-driven velocity $V \sim U/\lambda\epsilon^{1/2} \sim B^2\alpha$ becomes comparable with the rolling velocity . This occurs when $\lambda \sim B^{-1}$. Finally, if $\lambda \ll (B\alpha^2)^{-1/3}$, the drop slips and the film shear stress drives a passive internal flow of magnitude $V \sim U$ once again independent of λ.

In summary, on reducing λ from infinity, the internal flow velocity initially increases from zero (region CI_1), then is independent of λ when the drop is rolling slowly (region CI_2), increases again when the flow is shear driven (region CI_3), and becomes independent of λ again when the drop is sufficiently inviscid (region CI_4). An analogous double effect due to the viscosity ratio λ is seen for an infinitely long thread of fluid surrounded by a film in a cylindrical pipe (Hammond 1982): for large values of λ normal stresses are coupled and control the flow; for small values of λ it is the tangential stresses that drive the flow.

3.3.1. *Extension to finite wall slopes:* $\alpha \sim 1$, $B \ll 1$.

Although we have derived these near-circular results in the limit $\alpha \ll 1$, they remain valid for α of order unity, provided α is not close to $\pi/2$ so that the inclined plane is vertical. The layer thickness is $\epsilon \sim B^{-2/3} \ll 1$, and the drop speed $U \sim B^{-4/3} \ll 1$. The internal motion, V, scales as $B^{2/3}/\lambda$ when $\lambda \gg B^{-4/3}$; as B^2 when $B^{-1} \ll \lambda \ll B^{-4/3}$; and as $B^{4/3}$ when $\lambda \ll B^{-1/3}$.

4. Numerical coefficients for two-dimensional drops

Having established the scalings in table 1 and figure 4, we now determine the numerical coefficients in the leading-order scaling relations. We treat sliding and slipping motions for which the nose and tail regions do (§4.1) or do not (§4.2) overlap, near-circular drops (§4.3), tank-treading pancake-shaped drops (§4.4) and

rolling and slipping motions with a flat spot (§ 4.5). The only substantial region of parameter space that we do not treat in any detail is FII, since the entire internal flow within the drop needs to be computed in this case. Our analysis includes transitional behaviour at the boundaries between all regions outside FII, with the exception of the boundaries CI_3/CI_4 and $CI_2/FIII_1$. Numerical coefficients are summarized in table 2 in § 5 below.

4.1. *Sliding and slipping drops with overlapping nose and tail regions*

For sliding and slipping, the internal flow need not be calculated: we apply a no-slip or no-stress boundary condition for the film as appropriate. We start by examining such solutions here numerically, allowing the nose and tail regions to overlap, capturing the transitional regions CI_1/FI and $CI_4/FIII_2$ for which $B \sim \alpha$.

For sliding, the lubrication equations give the flow in the film as

$$u = \tfrac{1}{2}p_X(Z^2 - HZ) + (U/H)(Z - H) \quad \text{for} \quad 0 \leqslant Z \leqslant H(X), \tag{4.1}$$

so that $u = 0$ on $Z = H(X)$. Similarly, for slipping $u = \frac{1}{2}p_X(Z^2 - 2HZ) - U$, so that $u_Z = 0$ on $Z = H(X)$. The constant flux may be written in either case as

$$Q = -\tfrac{1}{3}(1+\chi)^{-2}p_X H^3 - (1+\chi)^{-1}UH \tag{4.2}$$

where $\chi = 1$ for sliding and $\chi = 0$ for slipping.

The pressure in the film is set by the interfacial curvature, so $P_d - p = H_{XX}$. In order to match to the outer sessile drop shape we must have

$$H \sim \tfrac{1}{2}P_d(X \mp L_d)^2 \quad \text{as} \quad X \to \pm\infty. \tag{4.3}$$

The normal force balance is then the static balance (2.7)

$$\int_{-\infty}^{\infty}(P_d - H_{XX})\,\mathrm{d}X = \pi B. \tag{4.4}$$

The weight tangential to the wall is supported by pressure and shear stresses

$$\int_{-\infty}^{\infty}(P_d - H_{XX})H_X\,\mathrm{d}X + \int_{-\infty}^{\infty}u_Z|_{Z=H}\,\mathrm{d}X = \pi B\alpha. \tag{4.5}$$

For both sliding and slipping, this may be written

$$\frac{1}{1+\chi}\left[P_d H - \tfrac{1}{2}H_X^2\right]_{-\infty}^{\infty} + \chi\int_{-\infty}^{\infty}UH^{-1}\,\mathrm{d}X = \pi B\alpha. \tag{4.6}$$

Using the scaling estimates given in table 1, we write $U = \alpha^3\mathscr{U}$, $Q = P_d^{-1}\alpha^5\mathscr{Q}$ and

$$H(X) = -(1+\chi)(Q/U)G(\xi), \quad X = -((1+\chi)^{2/3}U^4)^{1/3}Q\xi. \tag{4.7}$$

The film flux equation (4.2) becomes the Landau–Levich equation

$$G - G^3G_{\xi\xi\xi} = 1. \tag{4.8a}$$

The far-field behaviour is quadratic, and so

$$G \sim \begin{cases} \tfrac{1}{2}N_2\xi^2 + N_1\xi + N_0 + O(\xi^{-1}) & \text{as} \quad \xi \to \infty \quad \text{(nose)} \\ \tfrac{1}{2}T_2\xi^2 + T_1\xi + T_0 + O(\xi^{-1}) & \text{as} \quad \xi \to -\infty \quad \text{(tail).} \end{cases} \tag{4.8b}$$

The matching condition (4.3) gives

$$N_2 = T_2 = -((1+\chi)/9)^{1/3}\mathscr{Q}\mathscr{U}^{-5/3}, \quad N_1 = -T_1 = -\tfrac{1}{2}\pi(3(1+\chi))^{-1/3}\mathscr{U}^{-1/3}(B/\alpha), \tag{4.8c}$$

and the force balance (4.6) becomes

$$-\frac{\mathscr{Q}}{\mathscr{U}}(N_0 - T_0) + \frac{\chi}{2}\left(\frac{4}{3}\right)^{1/3}\mathscr{U}^{2/3}\Gamma = \pi\left(\frac{B}{\alpha}\right) \quad \text{where} \quad \Gamma = \int_{-\infty}^{\infty} G(\xi)^{-1}\,\mathrm{d}\xi. \qquad (4.8d)$$

We seek $\mathscr{U}$ and $G(\xi)$ as functions of B/α.

4.1.1. *Numerical results for CI_1/FI and $CI_4/FIII_2$*

The Landau–Levich equation (4.8*a*) was solved numerically by shooting to $\xi \to \pm\infty$ from $\xi = \xi_0$, with initial conditions $G_\xi = 0$ and prescribed values of G and $G_{\xi\xi}$. The unknown G and $G_{\xi\xi}$ at $\xi = \xi_0$ were determined using a Newton–Raphson method to satisfy the boundary conditions $N_2 = T_2$ and $N_1 = -T_1$ for each ξ_0. We were unable to find solutions for $\xi_0 < -5.8$ using this method because the solution is extremely sensitive to the initial value of G. We show in figure 6(*a*) the variation of N_2, N_1, $N_0 - T_0$ and Γ with ξ_0. Typical pressure distributions in the film are shown in figure 6(*b*). As ξ_0 is decreased, the pressure changes from that of a region-C drop (solid line) with near fore–aft symmetry towards a region-F drop (dashed lines) with a constant-pressure plateau below the flat spot. Equations (4.8*c*, *d*) determine B/α, $\mathscr{U}$ and $\mathscr{Q}$ in terms of ξ_0, and hence give $\mathscr{U}$ in terms of B/α.

For sliding ($\chi = 1$), $\mathscr{U}$ is plotted versus B/α in figure 7. For $B/\alpha \ll 1$ the result agrees with the asymptote $U = 2^{-8/3}(B^4\alpha^5)^{1/3}$ derived below (see (4.29)); the sliding speed is within 1% of this asymptote when $B/\alpha < 0.001$. For a drop with a distinct flat spot ($B/\alpha \gg 1$, region FI), $\mathscr{U}$ should reach a constant value as $B/\alpha \to \infty$ (see (4.12) below). It is evident from figure 7 that the numerical scheme broke down before $\mathscr{U}$ levels off, because we could not suppress exponentially growing terms over the flat base. As shown in figure 6(*b*) for $\xi_0 = -5.8$, the nose and tail are still not completely separated by a constant-pressure region, so the numerical solution shown in figure 7 does not approach its flat-spot limit for $B/\alpha \to \infty$. Nevertheless a numerical fit to the data in figure 6(*a*) indicates that as $\xi_0 \to -\infty$,

$$\Gamma \sim -2\xi_0 + 3.7, \quad N_1 \sim -0.7\xi_0 - 0.8, \quad N_2 \to 0.6, \quad N_0 - T_0 \to 3.6, \qquad (4.9)$$

giving the estimate $\mathscr{U} \approx 9.3$ as $B/\alpha \to \infty$, in fair agreement with the asymptote $\mathscr{U} = 9.57$ (see § 4.2 below). Extrapolation suggests that the sliding speed is within 10% of this asymptotic limit only for $B/\alpha \geqslant 400$.

A graph of $\mathscr{U}$ versus B/α for slipping ($\chi = 0$) is also plotted in figure 7. The results agree with the asymptotes $U = 0.497(B\alpha)^{3/2}$ for $B/\alpha \gg 1$ (see (4.15) below), and $U = 2^{-5/3}(B^4\alpha^5)^{1/3}$ for $B/\alpha \ll 1$ (see (4.30) below). The sliding speed is within 1% of these limits when $B/\alpha \geqslant 4$ (region $FIII_2$) and when $B/\alpha \leqslant 0.0001$ (region CI_4).

4.2. *Sliding and slipping drops with a flat spot*

If the drop has a distinct flat spot, then the nose and tail may be considered separately. Below the flat spot the film has uniform thickness ϵ, the pressure is uniform and so is the flux $Q = -\epsilon U/(1+\chi)$. The flux conservation equation (4.2) for the nose and tail becomes

$$-(1+\chi)^{-1}\epsilon U = \tfrac{1}{3}(1+\chi)^{-2}H_{XXX}H^3 - (1+\chi)^{-1}UH. \qquad (4.10)$$

For the nose we write $H = \epsilon G(\xi)$, $X = \frac{1}{2}L_d - \epsilon(3(1+\chi)U)^{-1/3}\xi$ and again obtain the Landau–Levich equation (4.8*a*). The boundary conditions are now

$$G \to 1 \text{ as } \xi \to -\infty, \quad G \to \tfrac{1}{2}N_2\xi^2 + N_0 + O(\xi^{-1}) \text{ as } \xi \to \infty. \qquad (4.11)$$

There is a unique solution satisfying these conditions (Bretherton 1961) for which $N_2 = \overline{N}_2 \approx 0.64304$, $N_0 = \overline{N}_0 \approx 2.89964$ (Jensen 2000). The matching condition (4.3)

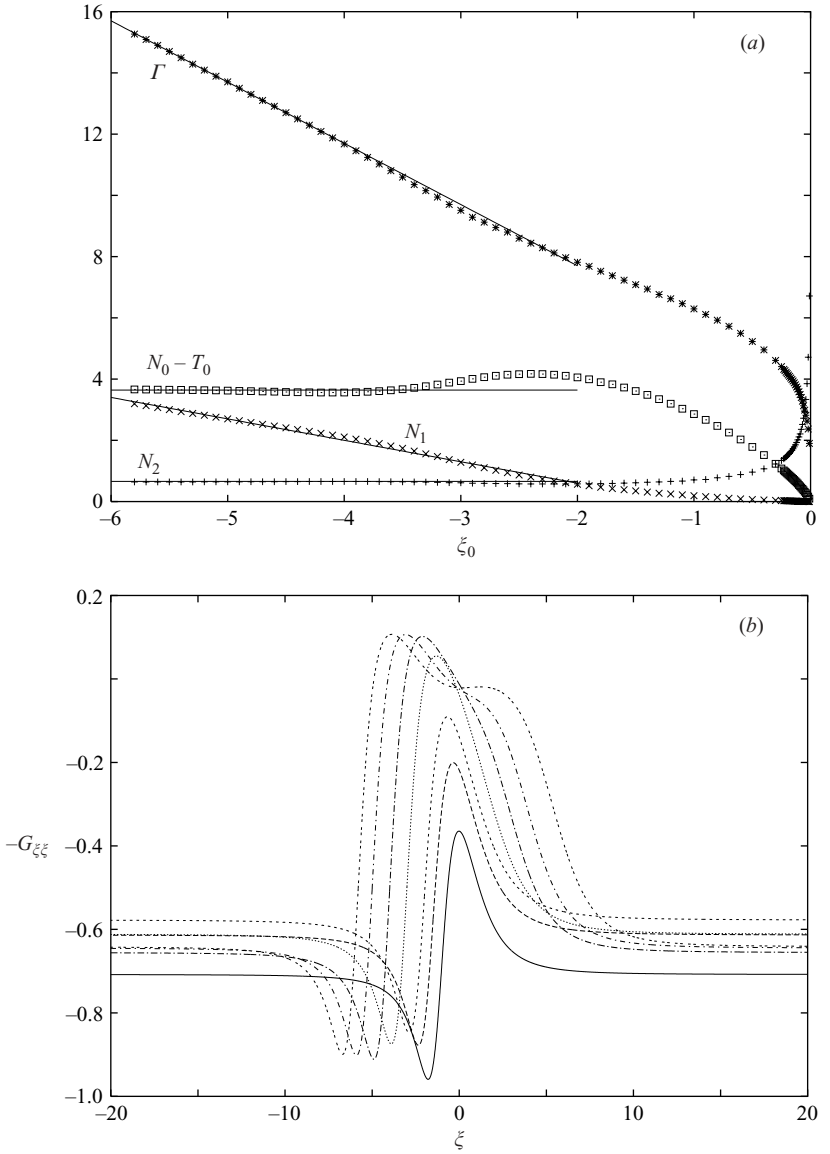

FIGURE 6. (*a*) Numerical solutions of (4.8*a–d*). Solid lines show the approximations in (4.9). (*b*) The pressure, $-G_{\xi\xi}(\xi)$, under a sliding or slipping drop for $\xi_0 = -1$ (solid line), -1.5, -2, -3, -4, -5, -5.8, obtained from (4.8*a–d*). The maximum pressure increases as ξ_0 is reduced.

requires $\epsilon P_d(3(1+\chi)U)^{-2/3} = \overline{N}_2$. This result is a Bretherton relation between drop speed and film thickness for a drop having nose curvature P_d. The two cases $\chi = 0$, $\chi = 1$ correspond respectively to an inviscid drop and to an infinitely viscous drop. We now use a force balance on the drop to determine U and ϵ.

4.2.1. *Sliding: regions FI, PI*

For sliding, the weight tangential to the wall is supported by shear forces along the flat spot, where the flow is Couette with $u = U(Z/\epsilon - 1)$. Thus $UL_d/\epsilon = \pi B\alpha$, giving

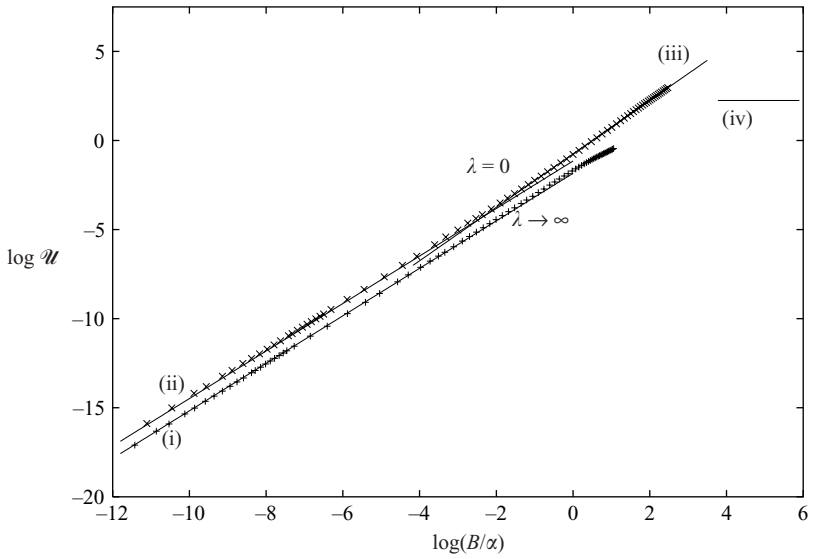

FIGURE 7. Numerical and asymptotic results for the drop speed for sliding ($\lambda \to \infty$) and slipping ($\lambda = 0$). The four solid lines are the asymptotes (i) $\frac{4}{3}\log(B/\alpha) - \frac{8}{3}\log 2$; (ii) $\frac{4}{3}\log(B/\alpha) - \frac{5}{3}\log 2$; (iii) $\frac{3}{2}\log(B/\alpha) + \log(0.497)$; (iv) $\log(9.57)$.

the sliding speed and film thickness as

$$U = 6^2\overline{N}_2^3\alpha^3 \approx 9.57\alpha^3, \quad \epsilon = 6^2\overline{N}_2^3\alpha^2/P_d \approx 9.57\alpha^2/P_d. \tag{4.12a,b}$$

As anticipated, the sliding speed U is independent of B, but the film thickness decreases with increasing B. In region FI, $P_d \approx 1$ in (4.12b). In region PI where $B \gg 1$, $P_d \approx 2B^{1/2}$ and therefore

$$\epsilon = \tfrac{1}{2}6^2\overline{N}_2^3 B^{-1/2}\alpha^2 \approx 4.79 B^{-1/2}\alpha^2. \tag{4.13}$$

Using numerically computed values of P_d (see figure 1b), (4.12) may also be used to describe the transition region FI/PI.

4.2.2. *Slipping: regions FIII$_2$, PIII*

The boundary conditions for the tail are $G \to 1$ as $\xi \to \infty$ and $G \to \frac{1}{2}T_2\xi^2 + T_0 + O(1/\xi)$ as $\xi \to -\infty$. The matching condition (4.3) requires $T_2 = \overline{N}_2$, and in this case the solution has $T_0 = \overline{T}_0 \approx -0.84529$ (Wong, Radke & Morris 1995). The tangential force balance for slipping (4.8d) reduces to

$$\epsilon P_d(\overline{N}_0 - \overline{T}_0) = \pi B\alpha, \tag{4.14}$$

giving the drop speed and film thickness as

$$U = \frac{1}{3}\left(\frac{\pi B\alpha}{\overline{N}_2(\overline{N}_0 - \overline{T}_0)}\right)^{3/2} \approx 0.497(B\alpha)^{3/2}, \quad \epsilon = \frac{\pi B\alpha}{P_d(\overline{N}_0 - \overline{T}_0)} \approx 0.839\frac{B\alpha}{P_d}. \tag{4.15a,b}$$

In region FIII$_2$, $P_d \approx 1$ in (4.15b). In region PIII where $B \gg 1$, $P_d \approx 2B^{1/2}$ and therefore

$$\epsilon = \tfrac{1}{2}\pi(\overline{N}_0 - \overline{T}_0)^{-1}B^{1/2}\alpha \approx 0.419 B^{1/2}\alpha. \tag{4.16}$$

Once again, (4.15) also applies across the transition region FIII$_2$/PIII.

It is straightforward to check that the couple balance is met by taking moments about the drop's centre of mass. Because the base is flat, the uniform pressure $P_d \approx 1$ below the flat spot exerts no net torque. The torque exerted by the pressure in the nose and tail is proportional to

$$\mathscr{T} = \int_{\text{Nose}} (1 - h_{xx})(x - h_x)\,\mathrm{d}x + \int_{\text{Tail}} (1 - h_{xx})(x - h_x)\,\mathrm{d}x \tag{4.17a}$$

$$= \left[\tfrac{1}{2}x^2 - xh_x + \tfrac{1}{2}h_x^2\right]_{\text{Nose}} + \left[\tfrac{1}{2}x^2 - xh_x + \tfrac{1}{2}h_x^2\right]_{\text{Tail}}. \tag{4.17b}$$

With boundary conditions $h \to \frac{1}{2}x^2 + h_0\overline{N}_0$, $h \to h_0$ as $x \to \pm\infty$ (for the nose) and $h \to h_0$, $h \to \frac{1}{2}x^2 + h_0\overline{T}_0$ as $x \to \pm\infty$ (for the tail), we find $\mathscr{T} = 0$.

4.3. *Sliding and slipping near-circular drops: regions CI_1–CI_4*

We now consider near-circular drops for which the nose, tail and flat spot merge, and apply a perturbation analysis to the lubrication theory of § 4.1. As shown in table 1, the appropriate scalings are

$$X = (B\alpha^2)^{1/3}\xi, \quad H(X) = (B\alpha^2)^{2/3}h(\xi), \quad U = (B^4\alpha^5)^{1/3}\mathscr{U}, \quad Q = B^2\alpha^3\mathscr{Q}. \tag{4.18}$$

The lubrication equations (4.2) for sliding ($\chi = 1$) and slipping ($\chi = 0$) become

$$(B/\alpha)^{1/3}\mathscr{Q} = -\tfrac{1}{3}(1+\chi)^{-2}p_\xi h^3 - (B/\alpha)^{1/3}(1+\chi)^{-1}\mathscr{U}h. \tag{4.19}$$

The pressure in the film is $1 - p = h_{\xi\xi}$. Because the drop base has no flat spot, the static normal force balance (2.2) no longer holds. Instead, the leading-order balance is

$$(B\alpha^2)^{1/3}\int_{-\infty}^{\infty} p(\xi)\,\mathrm{d}\xi = \pi B, \tag{4.20a}$$

and the tangential balance is

$$\frac{(B\alpha^2)^{2/3}}{1+\chi}\tfrac{1}{2}\left[h - \tfrac{1}{2}h_\xi^2\right]_{-\infty}^{\infty} + \chi B\alpha\mathscr{U}\int_{-\infty}^{\infty} h^{-1}\,\mathrm{d}\xi = \pi B\alpha. \tag{4.20b}$$

As described in § 3.3, we set $\varepsilon \equiv (B/\alpha)^{1/3} \ll 1$ and write

$$h(\xi) = h_0(\xi) + \varepsilon h_1(\xi) + O(\varepsilon^2)), \quad p(\xi) = \varepsilon p_1(\xi) + \varepsilon^2 p_2(\xi) + O(\varepsilon^3), \tag{4.21}$$

where the pressure $p_1(\xi)$ is an odd function of ξ and $p_2(\xi)$ is even. The force balances become

$$\int_{-\infty}^{\infty} p_2(\xi)\,\mathrm{d}\xi = \pi, \quad \frac{1}{1+\chi}[h_1 - h_{0\xi}h_{1\xi}]_{-\infty}^{\infty} + \chi\mathscr{U}\int_{-\infty}^{\infty} h_0^{-1}\,\mathrm{d}\xi = \pi. \tag{4.22a,b}$$

At leading order, $h_{0\xi\xi} = 1$ so that $h_0 = \frac{1}{2}(\xi^2 + \overline{\xi}^2)$, for some constant $\overline{\xi}$ that fixes the centre of the circular drop. At $O(\varepsilon)$, (4.19) becomes

$$\mathscr{Q} = -\tfrac{1}{3}(1+\chi)^{-2}p_{1\xi}h_0^3 - (1+\chi)^{-1}\mathscr{U}h_0. \tag{4.23}$$

There is no net change in p_1 from $\xi = -\infty$ to $\xi = \infty$, so that

$$\mathscr{Q} = -\tfrac{1}{3}\overline{\xi}^2\mathscr{U}(1+\chi)^{-1} \quad \text{and} \quad p_1 = -4(1+\chi)\mathscr{U}\xi(\xi^2 + \overline{\xi}^2)^{-2}. \tag{4.24}$$

As expected, p_1 is fore–aft anti-symmetric and supplies no contribution to the normal force. It does however perturb the drop shape, and because $p_1 = -h_{1\xi\xi}$ we find

$$h_1(\xi) = (2(1+\chi)\mathscr{U}/\overline{\xi})\tan^{-1}(\xi/\overline{\xi}). \tag{4.25}$$

Using h_0 and h_1 in the tangential force balance (4.22b) we obtain

$$(2\mathscr{U}\pi/\overline{\xi}) + \chi\mathscr{U}[(2/\overline{\xi})\tan^{-1}(\xi/\overline{\xi})]_{-\infty}^{\infty} = \pi, \tag{4.26}$$

and therefore the sliding speed is $\mathscr{U} = \frac{1}{2}(1+\chi)^{-1}\overline{\xi}$.

To satisfy the normal force balance and determine $\overline{\xi}$, we consider $O(\varepsilon^2)$. The second-order pressure satisfies the flux equation

$$-\tfrac{1}{3}(1+\chi)^{-1}p_{2\xi}h_0^3 - (1+\chi)^{-1}p_{1\xi}h_0^2h_1 - \mathscr{U}h_1 = 0, \tag{4.27}$$

and

$$\int_{-\infty}^{\infty} p_2(\xi)\,\mathrm{d}\xi = -\int_{-\infty}^{\infty}\xi p_{2\xi}\,\mathrm{d}\xi = \frac{\pi}{4\overline{\xi}^3}. \tag{4.28}$$

Thus the normal force balance (4.20a) gives $\overline{\xi} = 2^{-2/3}$, $\mathscr{U} = 2^{-5/3}/(1+\chi)$ and $\mathscr{Q} = -\frac{1}{12}(1+\chi)^{-2}$. The sliding speed and minimum film thickness for a near-circular sliding drop (cases $\mathrm{CI}_{1,2,3}$) are therefore

$$U = 2^{-8/3}(B^4\alpha^5)^{1/3}, \qquad \epsilon = 2^{-7/3}(B\alpha^2)^{2/3}, \tag{4.29}$$

while for a near-circular slipping drop (case CI_4),

$$U = 2^{-5/3}(B^4\alpha^5)^{1/3}, \qquad \epsilon = 2^{-7/3}(B\alpha^2)^{2/3}. \tag{4.30}$$

Thus, a sliding drop ($\mathrm{CI}_{1,2,3}$) moves half as fast as a slipping drop (CI_4). The film thicknesses are the same.

4.3.1. *Extension to finite wall slopes*

We noted that in region C the results for small α remain valid for $\alpha \sim 1$; the only changes that are needed to the calculation are the replacement of the tangential component of the drop weight $B\alpha$ by $B\sin\alpha$ and of the normal component by $B\cos\alpha$. Then for $B \ll 1$ the minimum film thickness and drop speed are

$$\epsilon = 0.198B^{2/3}\sin^{2/3}\alpha\tan^{2/3}\alpha, \quad U = 0.315B^{4/3}\sin^{4/3}\alpha\tan^{1/3}\alpha \tag{4.31a,b}$$

for slipping ($\lambda \ll B^{-1/3}$). For sliding, ($\lambda \gg B^{-1/3}$), U is a factor 2 smaller and the film thickness is unchanged.

4.4. *Tank-treading pancake drops: regions PI–PIII*

For pancake drops ($B \gg 1$) of intermediate viscosity, we can calculate the flow inside the drop as well as that in the film by using lubrication theory.

The flow in the film, away from the nose and tail regions, is $u = kZ - U$ for $0 \leqslant Z \leqslant \epsilon$, where the shear rate k is a constant. The associated shear stress drives an internal flow. There is no stress on the upper boundary $Z = H_d$ because the capillary number is small, and zero net flux of fluid inside the drop, so away from the ends the flow is given as

$$u = \tfrac{1}{2}(p_X/\lambda)\left(Z^2 - 2H_dZ + \tfrac{2}{3}H_d^2\right) \qquad \text{for} \qquad \epsilon \leqslant Z \leqslant H_d = 2B^{-1/2}. \tag{4.32}$$

Continuity of traction and velocity at the lower boundary $Z = \epsilon$ then give

$$p_X = -\frac{3UB\lambda}{4 + 6B^{1/2}\lambda\epsilon}, \quad k = \frac{6UB^{1/2}\lambda}{4 + 6B^{1/2}\lambda\epsilon}. \tag{4.33}$$

The tangential force balance (4.5) is

$$2B^{1/2}\epsilon(\overline{N}_0 - \overline{T}_0) + \tfrac{1}{2}\pi B^{1/2}k = \pi B\alpha, \tag{4.34}$$

giving the drop speed

$$U = \left(4 + 6B^{1/2}\lambda\epsilon\right)\left(\pi B\alpha - 2B^{1/2}\epsilon(\overline{N}_0 - \overline{T}_0)\right)/(3\pi B\lambda). \tag{4.35}$$

A second relationship between the sliding speed U and film thickness ϵ is given by the Bretherton problem determined in the nose. The curvature where the drop meets the wall is $P_d \approx 2B^{1/2}$, and Hodges *et al.* (2004) give $\epsilon = FP_d^{-1}U^{2/3}$ where the order-unity coefficient F is a function of λ and U having asymptotic behaviour

$$F \sim \begin{cases} F_0 \equiv 3^{2/3}\overline{N}_2 \approx 1.34, & \lambda \ll U^{-1/3}, \\ F_P \equiv 12^{2/3}\overline{N}_2 \approx 3.37, & U^{-1/3} \ll \lambda \ll U^{-2/3}, \\ F_\infty \equiv 6^{2/3}\overline{N}_2 \approx 2.12, & \lambda \gg U^{-2/3}. \end{cases} \tag{4.36}$$

Combining these results for U and ϵ, and neglecting a term $\lambda B^{-1}U^{4/3}$ that is always asymptotically small, we find

$$\lambda U - F\lambda\alpha U^{2/3} - \tfrac{4}{3}\alpha + \tfrac{4}{3}F(\pi B)^{-1}(\overline{N}_0 - \overline{T}_0)U^{2/3} = 0. \tag{4.37}$$

There are several possible balances in (4.37). For the sliding region (PI), the first and second terms balance and $U = F_\infty^3\alpha^3$, as in (4.12). For the slipping region (PIII), the third and fourth terms balance and U is as given in (4.15). For the tank-treading regions (PII_1 and PII_2), $(B^3\alpha)^{-1/2} \ll \lambda \ll \alpha^{-2}$ and $U \sim \alpha/\lambda$. Here the balance is between the first and third terms so that

$$U = \tfrac{4}{3}\alpha/\lambda \quad \text{and} \quad \epsilon = \tfrac{1}{2}FB^{-1/2}(4\alpha/3\lambda)^{2/3}. \tag{4.38}$$

In this limit, the shear rate in the film is (from (4.33))

$$k = \tfrac{3}{2}UB^{1/2}\lambda \tag{4.39}$$

which is independent of ϵ; it is controlled entirely by stress levels in the interior. Because the length of the flat spot is proportional to the drop weight, its speed is again independent of B. The transition between PII_1 and PII_2 occurs at $\lambda \sim \alpha^{-1/2}$. Here $\lambda U^{1/3}$ is comparable with unity and F changes from F_0 to F_P, so that $\epsilon \approx 0.812B^{-1/2}(\alpha/\lambda)^{2/3}$ in region PII_2 and $\epsilon \approx 2.04B^{-1/2}(\alpha/\lambda)^{2/3}$ in region PII_1. The transition in film thickness between regions PII_1 and PII_2 is plotted in figure 8(*a*), using the results for F from Hodges *et al.* (2004).

We may also determine transitional behaviour between other asymptotic regimes by keeping the relevant terms in (4.37) above. Thus, throughout regions PI and PII_1 (keeping the first three terms) we have

$$\lambda U - F\lambda\alpha U^{2/3} - \tfrac{4}{3}\alpha = 0. \tag{4.40}$$

The coefficient F varies between F_P and F_∞ across the transition where $\lambda U^{2/3}$ is order unity. Using the approximate result

$$F \approx F_\infty\left(\frac{2 + 4\lambda U^{2/3}F}{1 + 4\lambda U^{2/3}F}\right)^{2/3} \tag{4.41}$$

(Hodges *et al.* 2004) and rescaling $U = \mathscr{U}\alpha^3$, the speed $\mathscr{U}$ satisfies

$$\lambda\alpha^2\mathscr{U} - \lambda\alpha^2 F\mathscr{U}^{2/3} - \tfrac{4}{3} = 0, \quad \text{with} \quad F \approx F_\infty\left(\frac{2 + 4\lambda\alpha^2\mathscr{U}^{2/3}F}{1 + 4\lambda\alpha^2\mathscr{U}^{2/3}F}\right)^{2/3}. \tag{4.42}$$

Therefore $\mathscr{U}$ is a function of $\lambda\alpha^2$ only, consistent with table 1, and is plotted in figure 8(*b*). Both the speed and film thickness are within 10% of their respective asymptotic values whenever $\lambda\alpha^2 \leqslant 0.01$ (region PII_1) or $\lambda\alpha^2 \geqslant 2$ (region PI).

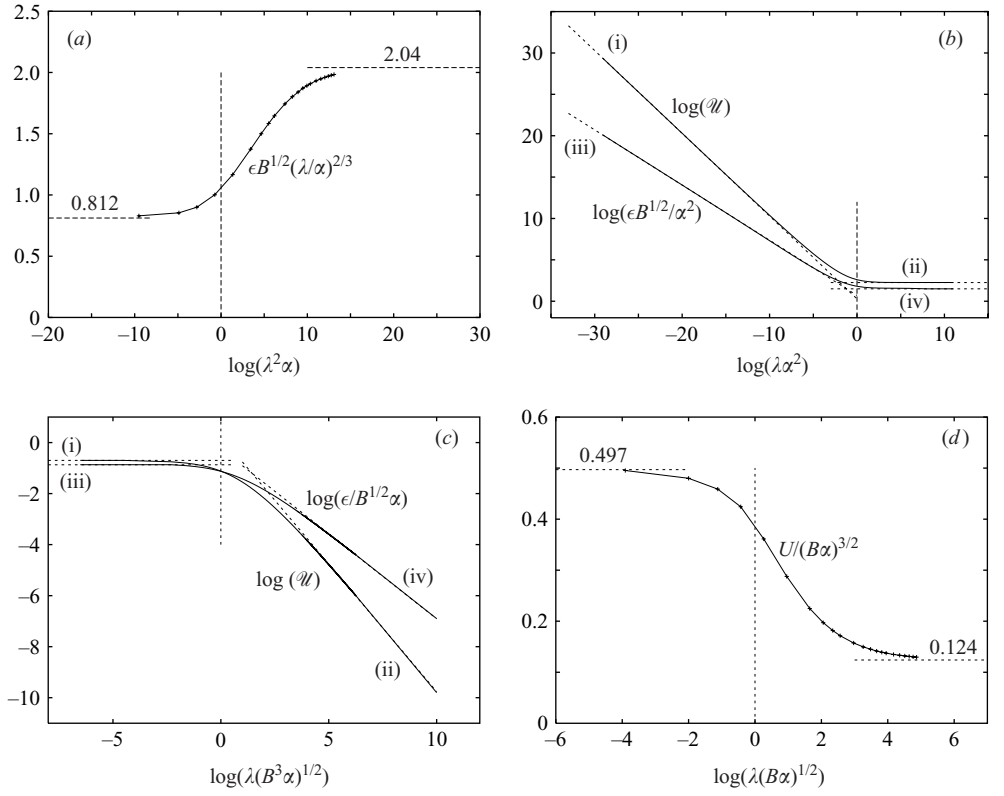

FIGURE 8. Film thickness and drop speed between regions: (*a*) PII_1 and PII_2; (*b*) PI and PII_1; (*c*) PIII and PII_2; (*d*) $FIII_1$ and $FIII_2$. The dotted lines show asymptotes as follows: in (*b*), (i) $\mathscr{U} = \frac{4}{3}\lambda\alpha^2$, (ii) $\mathscr{U} \approx 9.57$, (iii) $\epsilon B^{1/2}/\alpha^2 \approx 4.08/(\lambda\alpha^2)^{2/3}$, (iv) $\epsilon B^{1/2}/\alpha^2 \approx 4.79$; in (*c*), (i) $\mathscr{U} \approx 0.497$, (ii) $\mathscr{U} = \frac{4}{3}\lambda(B^3\alpha)^{1/2}$, (iii) $\epsilon/B^{1/2}\alpha \approx 0.419$, (iv) $\epsilon/B^{1/2}\alpha \approx 1.62/(\lambda(B^3\alpha)^{1/2})^{2/3}$.

In both regions PIII and PII_2, $\lambda \ll U^{-1/3}$ so that $F = F_0$. Throughout regions PIII and PII_2 the appropriate balance is (4.37) without its second term. In this case the rescaled velocity $\mathscr{U} = U/(B\alpha)^{3/2}$ depends only on $\lambda(B^3\alpha)^{1/2}$, consistent with table 1, and satisfies

$$\lambda(B^3\alpha)^{1/2}\mathscr{U} - \tfrac{4}{3} + \tfrac{4}{3}\pi^{-1}F_0(\overline{N}_0 - \overline{T}_0)\mathscr{U}^{2/3} = 0. \tag{4.43}$$

This drop speed $\mathscr{U}$ and film thickness are plotted in figure 8(*c*); both are within 10% of their respective asymptotic values whenever $\lambda(B^3\alpha)^{1/2} \leqslant 0.13$ (region PIII) or $\lambda(B^3\alpha)^{1/2} \geqslant 20$ (region PII_2).

4.5. *Rolling and slipping flat-spot drop: region FIII*

Throughout regions $FIII_1$ and $FIII_2$ the down-slope weight of the drop is supported by pressure in the nose and tail, as given by equation (4.14). Furthermore, for a flat-spot drop $P_d \approx 1$, and the relationship between the speed and film thickness is $\epsilon = FU^{2/3}$ (Hodges *et al.* 2004). It follows that the drop speed and film thickness are

$$U = (\pi B\alpha/F(\overline{N}_0 - \overline{T}_0))^{3/2}, \quad \epsilon = \pi B\alpha/(\overline{N}_0 - \overline{T}_0), \tag{4.44}$$

so the film thickness is independent of λ, given by that for slipping.

The slipping region $FIII_2$ has $\lambda \ll U^{-1/3}$ and therefore $F = F_0 = 3^{2/3}\overline{N}_2$. We recover the result (4.15) for U. On the other hand, for the rolling region $FIII_1$, $U^{-1/3} \ll \lambda \ll$

Region	Motion	Film thickness ϵ	Drop speed U
PI	Sliding	$4.79B^{-1/2}\alpha^2$	$9.57\alpha^3$
PII_1	Tank-treading	$2.04B^{-1/2}(\alpha/\lambda)^{2/3}$	$4\alpha/3\lambda$
PII_2	Slipping	$0.812B^{-1/2}(\alpha/\lambda)^{2/3}$	$4\alpha/3\lambda$
PIII	Slipping	$0.419B^{1/2}\alpha$	$0.497(B\alpha)^{3/2}$
FI	Sliding	$9.57\alpha^2$	$9.57\alpha^3$
$FIII_1$	Rolling	$0.839B\alpha$	$0.124(B\alpha)^{3/2}$
$FIII_2$	Slipping	$0.839B\alpha$	$0.497(B\alpha)^{3/2}$
$CI_{1,2,3}$	Sliding	$0.198(B\alpha^2)^{2/3}$	$0.157(B^4\alpha^5)^{1/3}$
CI_4	Slipping	$0.198(B\alpha^2)^{2/3}$	$0.315(B^4\alpha^5)^{1/3}$

TABLE 2. Asymptotes for film thickness and drop speed for a two-dimensional drop.

$U^{-2/3}$ and therefore $F = F_P = 12^{2/3}\overline{N}_2$ and the drop speed is $U = \frac{1}{12}(\pi B\alpha/\overline{N}_2(\overline{N}_0 - \overline{T}_0))^{3/2} \approx 0.124(B\alpha)^{3/2}$, a factor 4 slower.

The transition between regions $FIII_1$ and $FIII_2$ occurs when $\lambda \sim (B\alpha)^{-1/2}$. Here $\lambda U^{1/3}$ is order unity and F changes between F_0 and F_P. The drop speed across this transition may be computed using results from Hodges *et al.* (2004), as plotted in figure 8(*d*).

5. Two-dimensional drops: discussion

We have obtained expressions for the shape, film thickness and sliding speed of a two-dimensional drop as functions of B, α and λ in all the substantial regions of parameter space shown in figure 4, with the exception of FII. The asymptotes for the film thickness and drop speed are summarized in table 2. Furthermore, we have determined the transitional behaviour between different asymptotic regimes in all but a couple of cases. In FII energy is dissipated primarily inside the drop and three regions of disparate size must be taken into account; the flow field must be calculated throughout the entire drop, the geometry does not reduce to a half-plane. We have not pursued the boundary-integral calculation in this case.

To interpret these results it is helpful to consider some thought experiments. Suppose first that the drop size B and the inclination angle α are fixed but that the viscosity ratio λ is varied. Then a slipping drop (small λ) moves, with speed independent of λ, faster than a tank-treading or rolling drop (intermediate λ), with speed inversely proportional to λ. This speed is itself faster than a sliding drop (large λ), where again the speed becomes independent of λ.

Figure 9 shows schematically how the speed and film thickness vary with increasing B (i.e. with increasing drop size) and both λ and α fixed as we pass through distinct regions of parameter space. It is striking that the variation is not always monotonic. The results can be summarized as follows. As B is increased (so that the relative strength of gravity is increased), the drop travels faster, except when the drop adopts a tank-treading or sliding motion for which the speed is independent of B, or when the drop rolls and then, remarkably, the speed is reduced with B.

Finally, suppose that λ and B are fixed but that $\alpha \ll 1$ varies. Then, under all circumstances, the drop speed and the film thickness are monotically increasing functions of α — but having, rigorously, a nonlinear behaviour.

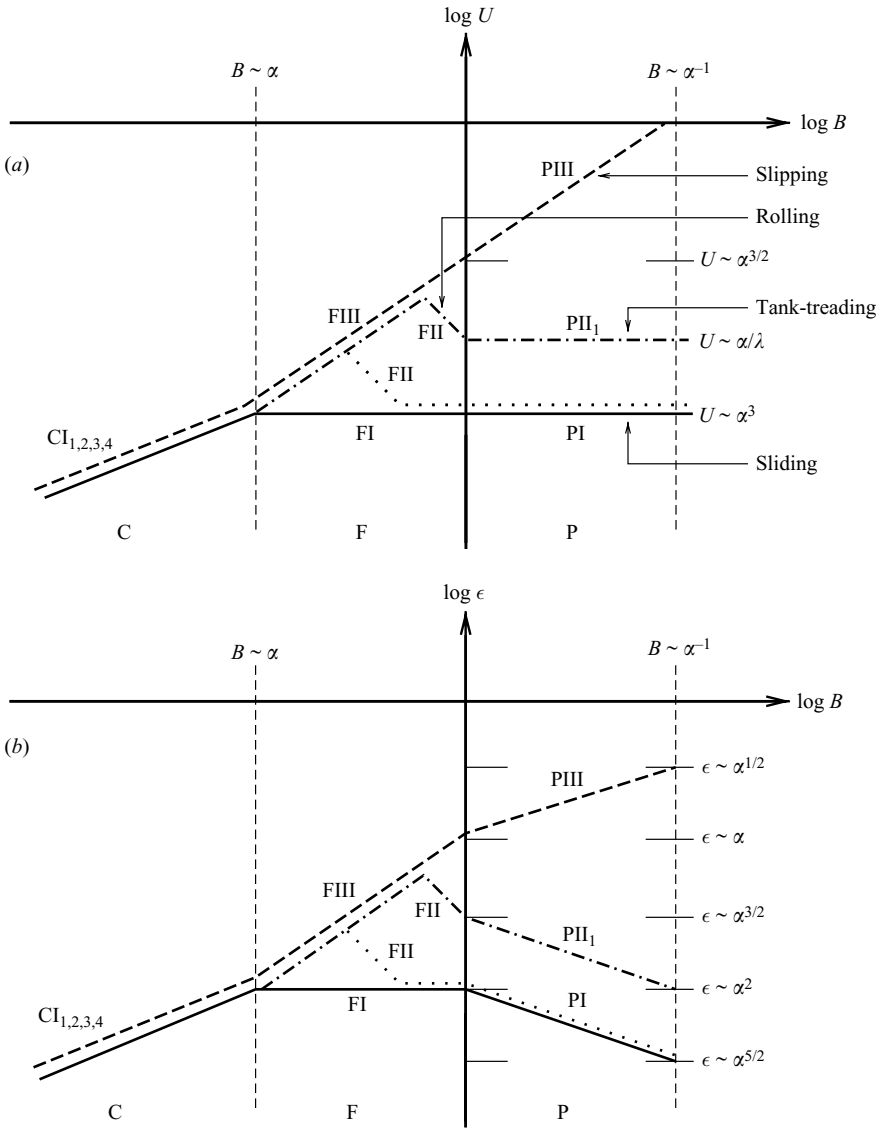

FIGURE 9. Depending on the size of λ (fixed), there are several ways of moving across phase space from small B to large B (see figure 4). Four possibilities are represented in the above sketch showing the scalings (on a logarithmic scale) for (*a*) speed U and (*b*) film thickness ϵ: (i) all sliding (solid line, $\lambda \gg \alpha^{-3}$); (ii) sliding–rolling–sliding (dotted line, $\alpha^{-2} \ll \lambda \ll \alpha^{-3}$); (iii) slipping–rolling–tank-treading (dotted and dashed line, $\alpha^{-1/2} \ll \lambda \ll \alpha^{-2}$); (iv) all slipping (dashed line, $\lambda \ll \alpha$).

5.1. *Comparison with computational studies*

DeBisschop *et al.* (2002) performed a numerical investigation of a periodic train of buoyant two-dimensional drops rising in an inclined channel. In terms of our variables, they considered $\lambda = 1$, $0.2 < B < 10$, a channel with width 2.2 and $0 \leqslant \alpha \leqslant \pi/2$. The smallest non-zero value for which explicit results were presented is $\alpha = \pi/9$. Unfortunately, much of their data have α too large for our asymptotic theory to be applicable because their effective capillary number is large enough for viscous forces to cause the drop shape to become strongly asymmetric away from the wall, and

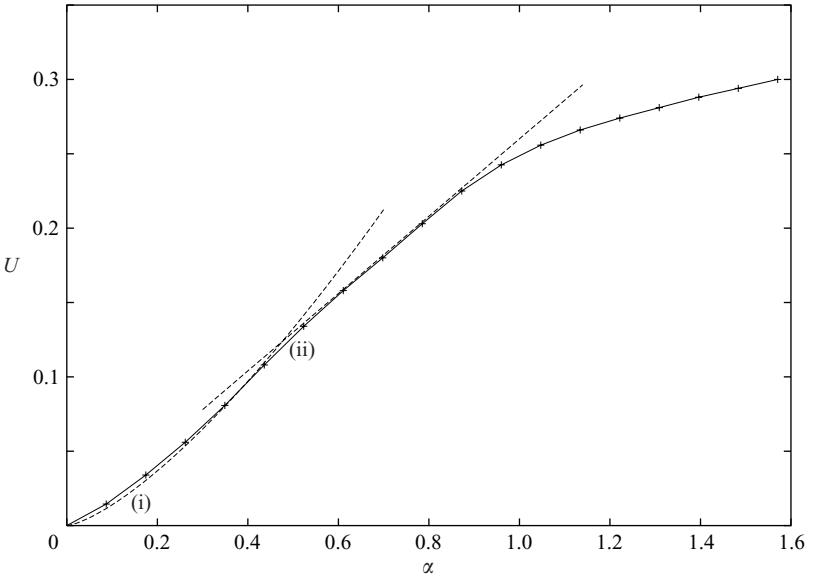

FIGURE 10. Symbols show drop speed with $B = 2.023$, $\lambda = 1$, as a function of channel inclination, taken from DeBisschop *et al.* (2002). Dotted lines show (i) $U = 0.4\alpha^{3/2}$ and (ii) $U = 0.3\alpha$.

sometimes large enough for no steady state to exist. However, for some parameters they found a steady drop translation speed with a film of near-uniform thickness between the drop and the upper channel wall. The film thickness increases with α. For the lowest value of $\alpha = 0.35$ and $B = 2.023$ (in our variables) they obtained a drop speed of $U = 0.089$ and a uniform film thickness $\epsilon = 0.11$. (The measured minimum film thickness 0.08 occurs in the tail and is about 70% of that under the flat spot). These values of B, α and λ have $\lambda(B^3\alpha)^{1/2} \approx 1.7$ and so set this example on the border between regions PIII and PII_2. As shown in figure 8(c) both the asymptotes for U and ϵ are too high, and the best estimate from the figure gives $U = 0.16$ and $\epsilon = 0.14$. We therefore over-predict the drop speed by around a factor 2, while the predicted film thickness is in better agreement. The discrepancy in U is most likely because the presence of the opposite wall of the channel in the computations of DeBisschop *et al.* increases the viscous drag on the main body of the bubble, slowing it down. Even so, their predictions of drop speed (reproduced in figure 10) are consistent with the scalings $U \sim (B\alpha)^{3/2}$ in region PIII (for small α) and $U \sim \alpha/\lambda$ in region PII_2 (for larger α), although the coefficients are about a factor 4 smaller than the asymptotic values in table 2.

DeBisschop *et al.* also give results for the drop speed and film thickness for $\alpha = \pi/3$, $\lambda = 1$ and varying B in the range [0.2, 3.03]. The small-B prediction for ϵ given by (4.31a) lies within a factor 2 throughout this range for B, and over-predicts the film thickness by about 50% for the smallest choice for B. The predicted slip velocity (4.31b) (slipping should be appropriate at the smaller values of B) is similarly too large, again by a factor about 2. Overall, however, agreement between the asymptotic predictions and simulations is encouraging.

6. Three-dimensional drops: scalings

We now extend the two-dimensional results to low-capillary-number sedimentation of three-dimensional drops. Once again, lengths are scaled on the radius a of the

undistorted drop, pressures on γ/a and speeds on μ/γ. Without going into as much detail as §§2 and 3, this Section gives an overview of the scalings governing three-dimensional drop motion, summarized in figure 12 and table 3 below. First, however, we recall the shape of a static drop resting on a plane.

6.1. *Sessile three-dimensional drop*

Consider an axisymmetric drop of volume $\frac{4}{3}\pi$ with shape given in cylindrical polar coordinates (r, θ, Z) by $Z = H(r)$. It sits on the plane $Z = 0$. Symmetry implies that at $r = 0$, $H_r = 0$. H_d is again the maximum height. The principal radii of curvature are

$$\kappa_r = \pm\frac{H_{rr}}{\left(1 + H_r^2\right)^{3/2}}, \quad \kappa_\theta = \pm\frac{1}{r}\frac{H_r}{\left(1 + H_r^2\right)^{1/2}}, \tag{6.1}$$

with signs changing at the turning point of the solution curve, and so the sessile drop shape is governed by the Young–Laplace equation and volume constraint

$$P_d - BH = \kappa_r + \kappa_\theta \quad \text{with} \quad \int_{\text{drop}} rH \, \mathrm{d}r = \tfrac{2}{3}. \tag{6.2}$$

We take zero contact angle at the wall so that $H_r = 0$ at $H = 0$. This condition is met at $r = L_d$ where L_d is the radius of the flat spot at the base. Note that because $H = \kappa_\theta = 0$ at the wall, the curvature κ_r at the wall is P_d. The static force balance (2.2) now becomes $P_d L_d^2 = \frac{4}{3}B$.

For $B \gg 1$ the drop has an axisymmetric pancake shape, with a flat top of height $H_d = P_d/B$. On the sides of the pancake, κ_θ is negligible, and thus the shape there is governed by the two-dimensional analysis of §2.1, giving

$$P_d = 2B^{1/2}, \quad H_d = 2B^{-1/2}, \quad L_d = \sqrt{\tfrac{2}{3}}B^{1/4}. \tag{6.3}$$

For $B \ll 1$ the drop is near-spherical and at leading order

$$P_d = 2, \quad H_d = 2, \quad L_d = \sqrt{\tfrac{2}{3}}B^{1/2}. \tag{6.4}$$

Mahadavan & Pomeau (1999) give different scalings but their result contains a typographical error. Rienstra (1990) gives more detailed asymptotic solutions using intrinsic coordinates. Experimental confirmation of the scalings for L_d in (6.3), (6.4) is provided by Aussillous & Quéré (2001, 2002).

6.2. *Three-dimensional sedimenting drops: lubrication theory*

We now suppose that the drop sediments in the X-direction (along $\theta = 0$) with velocity $\boldsymbol{U}$. Provided the capillary number is small (requiring (at least) that $U \ll 1$), the outer shape remains that of a sessile drop while the drop sediments, but the drop moves on a film of thickness of order ϵ. The film has a circular rim of width δ and circumference $2\pi L_d$ that takes the place of the two-dimensional nose and tail (as illustrated for a pancake-shaped drop in figure 11).

Suppose that the sedimenting drop has a distinct flat spot of radius $L_d \gg \delta$. The case where these lengths are comparable will be considered later. If the wall lies in the (X, Y)-plane, and the film thickness is $H(X, Y)$, then the interfacial curvature is $\nabla^2 H$, where $\nabla \equiv (\partial/\partial X, \partial/\partial Y)$. The flow in the film is governed by lubrication theory giving a steady flux $\boldsymbol{Q}$ in the (X, Y)-plane of the form

$$\boldsymbol{Q} = \beta_1 H^3 \nabla\nabla^2 H + \beta_2 \boldsymbol{U} H, \quad \text{with} \quad \nabla \cdot \boldsymbol{Q} = 0. \tag{6.5}$$

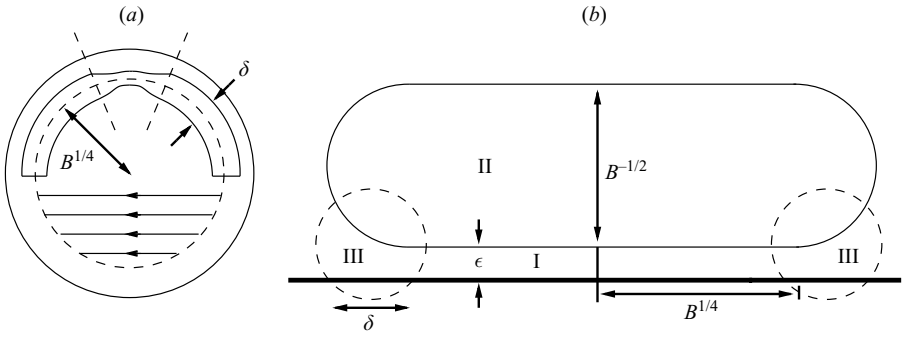

FIGURE 11. Sketch of a three-dimensional pancake drop ($B \gg 1$) showing (a) view from above, (b) view from the side. Also shown are relevant lengthscales (scaled on nominal drop radius a). The notation I, II, III indicates areas of primary potential energy dissipation.

The $O(1)$ coefficients β_1 and β_2 depend on λ. The first term arises from surface tension and is proportional to the gradient of the film curvature, the second is driven by the motion of the wall. Away from the rim, the ratio of the surface-tension-driven flux to that due to the motion of the wall scales as $(\epsilon/L_d)^3 U^{-1}$. Provided there is a distinct flat spot, this ratio is small, and (6.5) gives $\boldsymbol{U} \cdot \nabla H = 0$ and thus $H = H(Y)$. Thus the film thickness is approximately uniform from the front to the back of the drop and the corresponding flows in the film and the drop are unidirectional. In Neitzel & Dell'Aversana (2002) there is an image of an air film supporting an oil drop showing a region in which the film thickness is approximately independent of Y, although it does not extend across the entire base of the drop.

Because the rim has small width, over most of the rim radial derivatives are much larger than those in the circumferential direction, so the leading-order flux balance for the rim becomes

$$(\beta_1 H^3 H_{rrr} + \beta_2 U \cos\theta H)_r = 0. \tag{6.6}$$

This is a Landau–Levich equation (4.8a) for H, implying that the channel thickness is fixed locally at the leading edge of the rim where $r = L_d$ and $-\pi/2 < \theta < \pi/2$. Thus for the channel we recover the two-dimensional scalings (cf. (2.9))

$$\epsilon = H_d U^{2/3}, \quad \delta = H_d U^{1/3}. \tag{6.7}$$

Equivalently in these estimates H_d may be replaced by P_d^{-1}, because this is the curvature where a sessile drop meets the wall. A further consequence of (6.6) is that the channel thickness is proportional to $\cos^{2/3}\theta$, and hence $H(Y) \propto (1 - Y^2/L_d^2)^{1/3}$. Because H is non-uniform, the moving drop can no longer strictly be said to have a 'flat spot', although we retain this label. A representative film thickness ϵ is given by the value $H(0)$ at the mid-plane.

As discussed by Burgess & Foster (1990) for a drop in a Hele–Shaw cell, these scaling estimates cease to be valid in the regions of the rim where $Y \sim \pm L_d$, $\theta \sim \pm\pi/2$. In these rim-edge regions the circumferential flux term $r^{-1}(\beta_2 U \sin\theta h)_\theta$ becomes important. Putting $\theta = \pi/2 + \hat{\theta}$ with $\hat{\theta} \ll 1$, the leading-order Reynolds equation for this region becomes

$$(\beta_1 H^3 H_{rrr} - \beta_2 U \hat{\theta} H)_r - (\beta_2/L_d) U H_{\hat{\theta}} = 0. \tag{6.8}$$

Region	Motion	ϵ	L_d	δ	U	V	p
PI	Sliding	$B^{-1/2}\alpha^2$	$B^{1/4}$	$B^{-1/2}\alpha$	α^3	α/λ	$B^{1/2}$
PII_1	Tank treading	$B^{-1/2}(\alpha/\lambda)^{2/3}$	$B^{1/4}$	$B^{-1/2}(\alpha/\lambda)^{1/3}$	α/λ	α/λ	$B^{1/2}$
PII_2	Slipping	$B^{-1/2}(\alpha/\lambda)^{2/3}$	$B^{1/4}$	$B^{-1/2}(\alpha/\lambda)^{1/3}$	α/λ	α/λ	$B^{1/2}$
PIII	Slipping	$B^{1/4}\alpha$	$B^{1/4}$	$B^{-1/8}\alpha^{1/2}$	$(B^{3/4}\alpha)^{3/2}$	$(B^{3/4}\alpha)^{3/2}$	$B^{1/2}$
FI	Sliding	α^2	$B^{1/2}$	α	α^3	$\alpha/(B^{1/2}\lambda)$	1
FII	Rolling	$(\alpha^2/B\lambda^2)^{1/3}$	$B^{1/2}$	$B^{-1/6}(\alpha/\lambda)^{1/3}$	$\alpha/(B^{1/2}\lambda)$	$\alpha/(B^{1/2}\lambda)$	1
$FIII_1$	Rolling	$B^{1/2}\alpha$	$B^{1/2}$	$(B^{1/2}\alpha)^{1/2}$	$(B\alpha^2)^{3/4}$	$(B\alpha^2)^{3/4}$	1
$FIII_2$	Slipping	$B^{1/2}\alpha$	$B^{1/2}$	$(B^{1/2}\alpha)^{1/2}$	$(B\alpha^2)^{3/4}$	$(B\alpha^2)^{3/4}$	1
SI_1	Sliding	$B^{1/2}\alpha/\ln$	0	$(B^{1/2}\alpha/\ln)^{1/2}$	$B\alpha/\ln$	$1/\lambda$	$(B^{1/2}\ln/\alpha)^{1/2}$
SI_2	Rolling	$B^{1/2}\alpha/\ln$	0	$(B^{1/2}\alpha/\ln)^{1/2}$	$B\alpha/\ln$	$B\alpha/\ln$	$(B^{1/2}\ln/\alpha)^{1/2}$
SI_3	Slipping	$B^{1/2}\alpha/\ln$	0	$(B^{1/2}\alpha/\ln)^{1/2}$	$B\alpha/\ln$	$B\alpha/\ln$	$(B^{1/2}\ln/\alpha)^{1/2}$

TABLE 3. Scalings for a three-dimensional drop. Lengths are scaled on a, velocities on γ/μ and pressures on γ/a. For cases $SI_{1,2,3}$ the abbreviation ln stands for $\log(B^{-1}\alpha^{-2})$.

When all three terms in this equation are comparable, the scalings for the local film thickness $\hat{\epsilon}$, rim width $\hat{\delta}$ (satisfying $\hat{\delta} \sim (\epsilon H_d)^{1/2}$) and angular width $\hat{\theta}$ are

$$\hat{\epsilon} = H_d(H_d/L_d)^{2/5}U^{4/5}, \quad \hat{\delta} = H_d(H_d/L_d)^{1/5}U^{2/5}, \quad \hat{\theta} = (H_d/L_d)^{3/5}U^{1/5}. \tag{6.9}$$

Because the capillary number U is small, the rim-edge region has small angular width, $\hat{\theta}$, and the associated film thickness (proportional to $U^{4/5}$ rather than $U^{2/3}$ elsewhere) is especially small.

6.3. *Scaling estimates*

For a three-dimensional drop having $L_d \gg \delta$, there are thus four asymptotically distinct regions in which energy dissipation occurs: I, the channel under the flat spot of the sessile drop; II, the drop interior; III, the main part of the rim; and IV, the anomalous rim-edge described above (see figure 11).

The total dissipation in the rim-edge (region IV) scales as $\hat{\delta}(U/\hat{\epsilon})^2\hat{\epsilon}L_d\hat{\theta} = L_d(H_d/L_d)^{2/5}U^{9/5}$. The total dissipation elsewhere in the rim scales as $\delta(U/\epsilon)^2\epsilon L_d = L_dU^{5/3}$. The ratio of these estimates is $(H_d/L_d)^{2/5}U^{2/15}$ and this proves to be asymptotically small whenever $B \gg \alpha^2$. This is also the condition that $L_d \gg \delta$. It follows that the rim-edge region is dynamically passive: although the film is especially thin, with high shear rates, the spatial extent of region IV is sufficiently small that the associated dissipation is negligible. We note in passing however that the dangerously small power ($\frac{2}{15}$) of the small capillary number U may imply that our leading-order estimates are accurate only for unphysically small capillary numbers. We note too that the smallness of the rim-edge film thickness suggests that surface roughness may be important in experiments.

With these reservations we conclude that, for $B \gg \alpha^2$, the (B, λ)-parameter space for three-dimensional drops may be characterized on exactly the same basis as for two-dimensional drops, with different asymptotic regions labelled by F or P together with I, II or III depending upon the principal region of energy dissipation. The only differences in scaling behaviour are geometrical in character in moving from two to three dimensions.

The dissipation in the drop interior (region II) scales as $\lambda(V/H_d)^2 \sim \lambda V^2 B$ for tank treading ($B \gg 1$) and as $\lambda(L_dV/L_d)^2L_d^3 \sim \lambda V^2B^{3/2}$ for rolling ($B \ll 1$). Dissipation in the flat spot (region I) scales as $[(U-V)/\epsilon]^2\epsilon L_d^2$. Combining these estimates with those for the film thickness gives the scalings shown in table 3 and the parameter-space

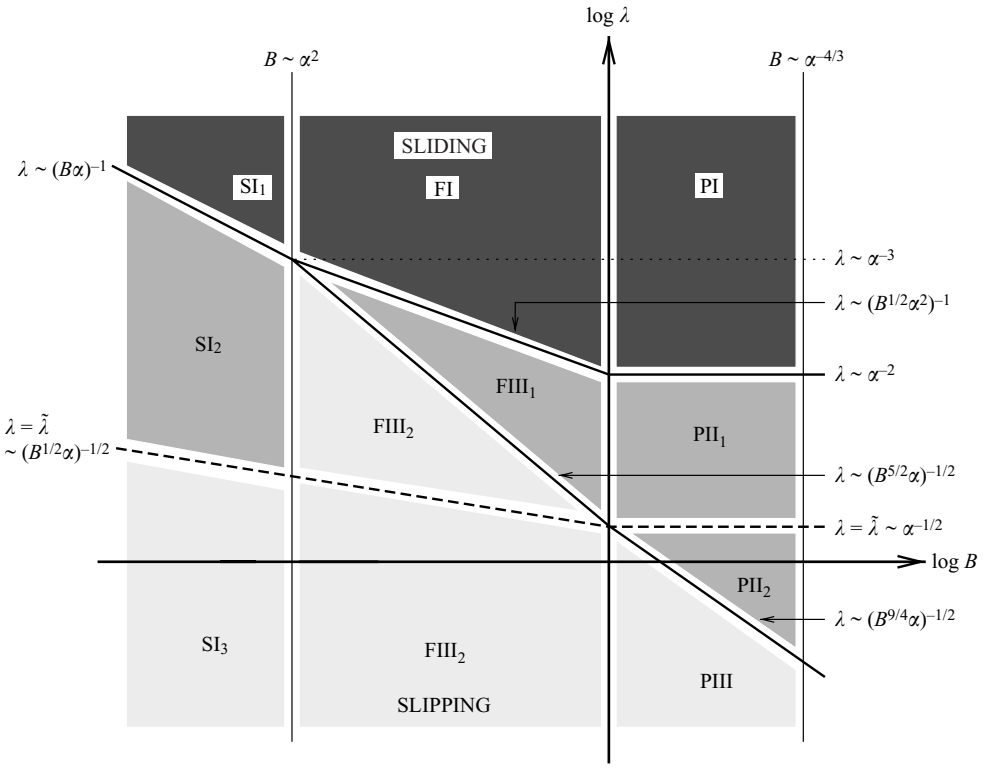

FIGURE 12. Sketch of (B, λ)-space for the three-dimensional drop, corresponding to scaling estimates given in table 3. In regions S the drop is near-spherical with a single region of deformation; in regions F the drop is near-spherical with a flattened disk on its base; in regions P the drop is pancake shaped. Dissipation occurs primarily in the channel in regions I; internally in regions II; to the fluid in the rim in regions III. The boundaries $\lambda \sim \tilde{\lambda}$ (dashed line) indicate when the interface rigidity in the rim is of order unity and provide an upper boundary for slipping. Logarithmic corrections to boundaries between SI_1, SI_2 and SI_3 have been ignored.

diagram in figure 12. Details are given in Hodges (2002). In particular we find that one or more of the capillary numbers U, λV and $\lambda B^{3/4} V$ cease to be small whenever $B \gg \alpha^{-4/3}$ so this provides an upper limit on B for our analysis to be appropriate. As anticipated above, whenever $B \lesssim \alpha^2$, the rim and flat-spot lengthscales become comparable and a more complex three-dimensional flow arises in the film. Scalings for regions SI_1–SI_3 are explained separately in § 7.2 below.

7. Numerical coefficients for three-dimensional drops

On recognizing that the channel flow and the rim flow are each two-dimensional, it is possible to adapt the estimates given in § 4 to provide three-dimensional results. We treat first regions F and P (§ 7.1) and then S (§ 7.2). The coefficients in the scaling relations for U and ϵ are summarized in table 4. We do not discuss FII, which requires a three-dimensional boundary-integral calculation that is beyond the scope of this paper, nor do we attempt to treat all the transitions between the dominant asymptotic domains.

Region	Motion	Film thickness ϵ	Drop speed U
PI	Sliding	$3.54B^{-1/2}\alpha^2$	$6.11\alpha^3$
PII_1	Tank-treading	$1.69B^{-1/2}(\alpha/\lambda)^{2/3}$	$4\alpha/3\lambda$
PII_2	Slipping	$0.670B^{-1/2}(\alpha/\lambda)^{2/3}$	$4\alpha/3\lambda$
PIII	Slipping	$0.407B^{1/4}\alpha$	$0.474(B^{3/4}\alpha)^{3/2}$
FI	Sliding	$3.54\alpha^2$	$6.11\alpha^3$
$FIII_1$	Rolling	$1.026B^{1/2}\alpha$	$0.119(B\alpha^2)^{3/4}$
$FIII_2$	Slipping	$0.407B^{1/2}\alpha$	$0.474(B\alpha^2)^{3/4}$
SI_1	Sliding	$\frac{1}{4}\sqrt{2}\,B^{1/2}\alpha/\ln$	$\frac{5}{6}B\alpha/\ln$
SI_2	Rolling	$\frac{1}{6}\sqrt{2}\,B^{1/2}\alpha/\ln$	$\frac{4}{9}B\alpha/\ln$
SI_3	Slipping	$\frac{1}{6}\sqrt{2}\,B^{1/2}\alpha/\ln$	$\frac{10}{9}B\alpha/\ln$

TABLE 4. Asymptotes for mid-plane film thickness and drop speed for a three-dimensional drop. Here $\ln \equiv \log(B^{-1}\alpha^{-2})$.

7.1. *Numerical coefficients for flat-spot and pancake drops*

7.1.1. *Sliding: regions FI, PI*

For sliding, the channel thickness is $H(Y) = F_\infty U^{2/3} P_d^{-1}(1-Y^2/L_d^2)^{1/3}$, with the coefficient F_∞ given by (4.36). The flow in the channel is Couette so that $\boldsymbol{u} = \boldsymbol{U}(1-Z/H)$ and the tangential force balance becomes

$$\int\!\!\int \frac{U}{H} r \,\mathrm{d}r\,\mathrm{d}\theta = \tfrac{4}{3}\pi B\alpha. \tag{7.1}$$

On performing the integration we find that $U = k\alpha^3$ where $k = (\pi F_\infty/4J)^3$ and $J \equiv \int_0^{\pi/2} \cos^{4/3}\theta\,\mathrm{d}\theta \approx 0.911$, so that $k \approx 6.11$. As in the corresponding two-dimensional case, U is independent of B: as the drop weight increases so, in proportion, does the area of the base and so also the viscous resistance from the channel flow. The corresponding mid-plane film thickness is

$$\epsilon = F_\infty k^{2/3}\alpha^2/P_d \approx 7.08\alpha^2/P_d. \tag{7.2}$$

This varies with drop size, having limiting behaviours in FI and PI shown in table 4. One may use numerically computed values of the capillary pressure P_d for $B = O(1)$ in (7.2) to describe behaviour on the FI/PI boundary.

7.1.2. *Slipping: regions $FIII_2$, PIII*

For slipping, the channel thickness is $H(Y) = F_0 U^{2/3} P_d^{-1}(1 - Y^2/L_d^2)^{1/3}$ with the coefficient F_0 given by (4.36). In particular near the rim, $H = F_0 U^{2/3} P_d^{-1}\cos^{2/3}\theta$. The force balance (4.14) is now provided by the difference between the X-component of the pressure force on the front and rear of the rim so that

$$\int_{-\pi/2}^{\pi/2} H(\overline{N}_0 - \overline{T}_0) P_d L_d \cos\theta\,\mathrm{d}\theta = \tfrac{4}{3}\pi B\alpha. \tag{7.3}$$

We obtain

$$U = \left(\frac{P_d B}{3}\right)^{3/4}\left(\frac{\pi}{F_0(\overline{N}_0 - \overline{T}_0)K}\right)^{3/2}\alpha^{3/2} \quad \text{and} \quad \epsilon = \left(\frac{B}{3P_d}\right)^{1/2}\frac{\pi\alpha}{(\overline{N}_0 - \overline{T}_0)K}, \tag{7.4}$$

where $K \equiv \int_0^{\pi/2} \cos^{5/3}\theta \, \mathrm{d}\theta \approx 0.841$. Limiting expressions for U and ϵ in PIII and FIII_2 are given in table 4. Once again, since P_d is readily determined numerically for $B = O(1)$, (7.4) applies also on the FIII_2/PIII boundary.

7.1.3. *Tank-treading: regions PII_1 and PII_2*

For a tank-treading pancake drop, the tangential component of the weight is supported by shear stresses in the film, and these are themselves determined by the shear stress in the drop interior. The near-uniform drop height H_d is $2B^{-1/2}$ for both two-dimensional and axisymmetric drops and the flow in the film and in the drop interior is unidirectional in both cases. In consequence the thin-film shear-rate independent of Y is given by (4.39) as $3\lambda U B^{1/2}/2$. The corresponding shear stress acts in the X-direction over the base to give

$$\tfrac{3}{2}\lambda U B^{1/2}\pi L_d^2 = \tfrac{4}{3}\pi B\alpha, \tag{7.5}$$

and hence $U = 4\alpha/3\lambda$, as for a two-dimensional drop. The corresponding channel thickness at the mid-plane is $\epsilon = \frac{1}{2}FU^{2/3}B^{-1/2}$, where the coefficient F is F_0 for slipping (region PII_2) and F_P for tank-treading (region PII_1). Limiting expressions for ϵ in PII_1 and PII_2 are given in table 4. The transitional behaviour on $\mathrm{PII}_1/\mathrm{PII}_2$ may be determined (as in two dimensions, see figure 8*a*) using the results of Hodges *et al.* (2004).

7.1.4. *Rolling and slipping drop: region FIII*

For a flat-spot drop having $P_d \approx 2$, the relationship between the speed and film thickness is $\epsilon = \frac{1}{2}FU^{2/3}$. Throughout regions FIII_1 and FIII_2 the down-slope weight is supported by pressure in the nose and tail. Thus just as for two-dimensional drops (§ 4.5), the film thickness is independent of λ, and is therefore given by that for slipping as calculated above.

Region FIII_2 has $\lambda \ll U^{-1/3}$ and therefore $F = F_0 = 3^{2/3}\overline{N}_2$. On the other hand, for the rolling region FIII_1, $U^{-1/3} \ll \lambda \ll U^{-2/3}$ and therefore $F = F_P = 12^{2/3}\overline{N}_2$ and so the drop speed is a factor 4 slower, and the film thickness a factor $4^{2/3}$ larger, as shown in table 4.

7.2. *Near-spherical drop with no flat spot*

Finally, we turn to regions SI_1–SI_3. The circumference of the rim L_d and its width δ are comparable when $B \lesssim \alpha^2$. Cases S, for which $B \ll \alpha^2$, correspond to a drop which is nearly spherical everywhere except for a single region of deformation at its base with radius $\epsilon^{1/2}$. We derive scalings in § 7.2.1 (the three-dimensional analogue of § 3.3) and then compute leading-order coefficients in § 7.2.2 (the analogue of § 4.3).

7.2.1. *Scaling estimates*

When $B \ll \alpha^2$, there is a high pressure in the film in front of the drop and a low pressure behind. To maintain a steady flux, the pressure difference between the front and rear scales as $p_1 \sim U/\epsilon^{3/2}$. This pressure contributes a tangential force on the drop which supports its down-slope weight, $B\alpha$. At first sight this appears to give $B\alpha \sim (U/\epsilon^{3/2})\epsilon^{1/2}(\epsilon^{1/2})^2 = U$, but this estimate requires amendment because the integral for the force decays as r^{-1} and must be truncated as $r \to \infty$ at a dimensionless distance ϵ^{-1}. Instead, the tangential force is $U\log\epsilon^{-1}$ and thus $U \sim B\alpha/\log\epsilon^{-1}$. The contribution to this force from shear over the base is no larger than this estimate and so the scaling for U is independent of λ. We note that the Stokes drag acting on the

main body of the drop provides an $O(B\alpha)$ correction to U and, except for extremely small values of ϵ, this is likely to be numerically significant.

As in two dimensions, the pressure p_1 is fore–aft anti-symmetric and exerts no net force in the direction normal to the wall. Instead, it deforms the drop radius by an amount $d = U\epsilon^{-1/2}$ against surface tension (so that the relative deformation is $U/\epsilon^{3/2}$). The corresponding change in lubrication pressure is fore–aft symmetric and has magnitude $p_2 \sim U^2/\epsilon^3$. This supports the drop weight so that $B \sim U^2\epsilon^{-3}(\epsilon^{1/2})^2$. Thus $\epsilon \sim B^{1/2}\alpha/\log(B^{-1}\alpha^{-2})$, $p_1 \sim (B^{1/2}\log(B^{-1}\alpha^{-2})/\alpha)^{1/2}$ and $p_2 \sim B^{1/2}\log(B^{-1}\alpha^{-2})/\alpha$.

We now consider the scaling for the internal flow. For $\lambda \to 0$ (region SI_1), the drop slips and the flow in the film drives a passive internal flow with magnitude $V \sim U$. As λ increases, the internal fluid resists this stirring and, when the interface rigidity $\lambda\epsilon^{1/2}$ of the base is of order unity, i.e. when $\lambda \sim (B^{1/2}\alpha/\log(B^{-1}\alpha^{-2}))^{-1/2}$, the internal viscosity no longer permits velocity variations over the base, slipping ceases and the drop rolls (region SI_2). The internal flow is rigid-body rotation together with a perturbation flow in a region of length $\epsilon^{1/2}$ near the base. The velocity of the rigid-body rotation is determined by a couple balance. For very large λ (region SI_1), because the drop is not perfectly spherical it slides with only a sluggish internal motion, $V \ll U$. The perturbation flow near the drop base has magnitude $Vd\epsilon^{-1/2}$ which generates internal stresses of magnitude $\lambda Vd\epsilon^{-1}$. Balancing normal stresses at the lower boundary (i.e. balancing with p_1) we find that $V \sim 1/\lambda$.

Table 3 summarizes these scalings. The boundaries between regions SI_1 and SI_2 (at $\lambda \sim (B\alpha)^{-1}$) and between regions SI_2 and SI_3 (at $\lambda \sim (B^{1/2}\alpha)^{-1/2}$) are shown in figure 12 (neglecting logarithmic corrections). We now determine the coefficients in these scaling relations.

7.2.2. *Numerical values*

For a drop that is sliding, or rolling with velocity $\boldsymbol{V}$, the lubrication equations give the flow in the film in $0 \leqslant Z \leqslant H$ as $\boldsymbol{u} = \frac{1}{2}\nabla p(Z^2 - HZ) + (\boldsymbol{U} - \boldsymbol{V})(Z/H) - \boldsymbol{U}$, where $\boldsymbol{u} = -\boldsymbol{U} \equiv -\mathscr{U}\boldsymbol{e}_X$ on $Z = 0$ and $\boldsymbol{u} = -\boldsymbol{V} \equiv -\mathscr{V}\boldsymbol{e}_X$ on $Z = H$, with $\mathscr{U} > 0$ and $\mathscr{V} > 0$. For slipping, with $\boldsymbol{u}_Z = 0$ on $Z = H$, $\boldsymbol{u} = \frac{1}{2}\nabla p(Z^2 - 2HZ) - \boldsymbol{U}$. The flux may be written in all three cases as

$$\boldsymbol{Q} = -\tfrac{1}{3}(1+\chi)^{-2}H^3\nabla p - (1+\chi)^{-1}(\boldsymbol{U} + \chi\boldsymbol{V})H \tag{7.6}$$

where $\chi = 1$ and $\boldsymbol{V} = 0$ for sliding; $\chi = 1$ and $\boldsymbol{V}$ is determined by a couple balance for rolling; and $\chi = 0$ for slipping. Reynolds' equation $\nabla\cdot\boldsymbol{Q} = 0$ is then

$$\nabla\cdot(H^3\nabla p) = -3(1+\chi)(\boldsymbol{U} + \chi\boldsymbol{V})\cdot\nabla H. \tag{7.7}$$

The pressure in the film is set by the curvature, so $P_d - p = \nabla^2 H$, where $P_d = 2$ to leading order.

Omitting for the present the anticipated logarithmic correction, the appropriate scalings are

$$r = \left(B^{1/2}\alpha\right)^{1/2}\rho, \quad H(r,\theta) = \left(B^{1/2}\alpha\right)h(\rho,\theta), \quad U = B\alpha\mathscr{U}, \quad V = B\alpha\mathscr{V}, \tag{7.8}$$

and setting $\varepsilon \equiv (B^{1/2}/\alpha)^{1/2}$, (7.7) becomes

$$\nabla\cdot(H^3\nabla p) = -3\varepsilon(1+\chi)(\mathscr{U} + \chi\mathscr{V})\boldsymbol{e}_X\cdot\nabla H, \tag{7.9}$$

where ∇ is defined with respect to ρ and $\boldsymbol{e}_X$ points along $\theta = 0$. These scalings, along with the self-evident angular dependences, enable us to write

$$h(\rho,\theta) = h_0(\rho) + \varepsilon h_1(\rho)\cos\theta + O(\varepsilon^2), \tag{7.10a}$$

$$p(\rho,\theta) = \varepsilon p_1(\rho)\cos\theta + \varepsilon^2[p_2(\rho) + p_2'(\rho)\cos 2\theta] + O(\varepsilon^3). \tag{7.10b}$$

At leading-order, $\nabla^2 h_0 = 2$ so that $h_0 = \frac{1}{2}(\rho^2 + \overline{\rho}^2)$, for some constant $\overline{\rho}$ that fixes the centre of the spherical drop. Corrections to P_d arising from the constant-volume constaint in the drop are $O(\varepsilon^2)$ and may be neglected in what follows.

At $O(\varepsilon)$, (7.9) gives

$$\rho\left(\rho h_0^3 p_{1\rho}\right)_\rho - h_0^3 p_1 = -3(1+\chi)(\mathscr{U} + \chi\mathscr{V})\rho^3. \tag{7.11}$$

The only acceptable decaying solution is (O'Neill & Stewartson 1967)

$$p_1 = \tfrac{12}{5}(1+\chi)(\mathscr{U} + \chi\mathscr{V})\rho(\rho^2 + \overline{\rho}^2)^{-2}. \tag{7.12}$$

Because the leading-order pressure is proportional to $\cos\theta$, it supplies no contribution to the normal force. It perturbs the drop shape, and because $p_1 \cos\theta = -\nabla^2(h_1 \cos\theta)$ we find

$$h_1 = \tfrac{3}{5}(1+\chi)(\mathscr{U} + \chi\mathscr{V})\rho^{-1}\log(1 + \rho^2/\overline{\rho}^2). \tag{7.13}$$

To satisfy the normal force balance we consider $O(\varepsilon^2)$ terms in (7.9). Only the term independent of $\cos 2\theta$ can provide a net force. This second-order pressure $p_2(\rho)$ satisfies

$$\left(\rho h_0^3 p_{2\rho}\right)_\rho = -\tfrac{3}{2}\left(\rho h_0^2 h_1 p_{1\rho}\right)_\rho - \tfrac{3}{2}(1+\chi)(\mathscr{U} + \chi\mathscr{V})(\rho h_1)_\rho \tag{7.14}$$

and p_2 is bounded as $\rho \to 0$. The normal force is then

$$2\pi \int_0^\infty p_2 \rho \, \mathrm{d}\rho = -\pi \int_0^\infty \rho^2 p_{2\rho} \, \mathrm{d}\rho = \frac{6\pi}{25\overline{\rho}^4}(1+\chi)^2(\mathscr{U} + \chi\mathscr{V})^2 = \frac{4\pi}{3}. \tag{7.15}$$

It follows that the minimum gap thickness is

$$\epsilon = \tfrac{1}{2}\overline{\rho}^2 B^{1/2}\alpha = (3\sqrt{2}/20)(1+\chi)(\mathscr{U} + \chi\mathscr{V})B^{1/2}\alpha. \tag{7.16}$$

For slipping ($\chi = 0$), there is no shear stress, and the tangential force balance on the drop gives

$$\iint p_1 h_{0\rho} \cos^2\theta \rho \, \mathrm{d}\rho \, \mathrm{d}\theta = \frac{12\pi\mathscr{U}}{5} \log\epsilon^{-1} = \tfrac{4}{3}\pi. \tag{7.17}$$

For sliding ($\chi = 1, \mathscr{V} = 0$), the shear stress on the boundary gives a total tangential force (O'Neill & Stewartson 1967)

$$\iint \left[p_1 h_{0\rho} \cos^2\theta + \tfrac{1}{2} h_0 \left(p_{1\rho} \cos^2\theta + \frac{p_1}{\rho} \sin^2\theta \right) + \frac{\mathscr{U}}{h_0} \right] \rho \, \mathrm{d}\rho \, \mathrm{d}\theta = \frac{16\pi\mathscr{U}}{5} \log\epsilon^{-1} = \tfrac{4}{3}\pi. \tag{7.18}$$

For rolling ($\chi = 1$), the velocity $\mathscr{V}$ must be chosen so as to provide no net couple on the drop. Pressure forces exert no couple about the centre of a spherical drop, and thus the net couple due to shear forces, which is itself proportional to the total shear force, must vanish. The shear force is

$$\iint \left[\tfrac{1}{2} h_0 \left(p_{1\rho} \cos^2\theta + \frac{p_1}{\rho} \sin^2\theta \right) + \frac{\mathscr{U} - \mathscr{V}}{h_0} \right] \rho \, \mathrm{d}\rho \, \mathrm{d}\theta = 0, \tag{7.19}$$

giving $\mathscr{V} = \mathscr{U}/4$ (Goldman *et al.* 1967). The tangential force balance is then

$$\iint p_1 h_{0\rho} \cos^2\theta \rho \, \mathrm{d}\rho \, \mathrm{d}\theta = 6\pi\mathscr{U} \log\epsilon^{-1} = \tfrac{4}{3}\pi. \tag{7.20}$$

The resulting expressions for U and ϵ for near-spherical slipping, rolling and sliding drops in cases SI_1–SI_3 are shown in table 4.

7.2.3. *Extension to finite wall slopes*

For regions S the results for small α remain valid for $\alpha \sim 1$; the only changes that are needed to the calculation are the replacement of the tangential component of the drop weight $4B\alpha/3$ by $4B\sin\alpha/3$ and of the normal component by $4B\cos\alpha/3$. For sliding the relevant parameter range is $\lambda \gg B^{-1}$, for rolling $B^{-1/4} \ll \lambda \ll B^{-1}$ and for slipping $\lambda \ll B^{-1/4}$. Thus for $B \ll 1$, the drop speed and minimum film thickness are

$$U = k_1 B \sin\alpha / \log B^{-1}, \quad \epsilon = k_2 B^{1/2} \sin^{1/2}\alpha \tan^{1/2}\alpha / \log B^{-1}, \tag{7.21}$$

where $k_1 \approx (0.833, 0.444, 1.11)$ and $k_2 \approx (0.353, 0.236, 0.236)$ for sliding, rolling and slipping respectively.

8. Three-dimensional drops: discussion

8.1. *Experiments*

We now consider our results in the light of the small number of available experiments treating low-Reynolds-number motion of non-wetting drops and bubbles in the neighbourhood of a gently inclined plane.

Tsao & Koch (1997) measured a drag coefficient $C_D \approx 100/Re$ of a bubble rising near a plane for $Re \approx 45$–200, which in our notation is equivalent to $U \approx (2/75)B\sin\alpha$. Although α is not small in their experiments, this is broadly consistent with predictions in SI_3. They report $B = O(10^{-2})$, which is not small enough to match quantitatively with (7.21) with $k_1 \approx 1.11$. This reflects the poor (logarithmic) accuracy of this prediction and the potential importance of inertia in their experiments.

Richard & Quéré (1999) observed glycerol droplets moving over an inclined superhydrophobic fibrous surface in air under the action of gravity. They used a viscous, nearly non-wetting liquid (with a contact angle close to but less than π). Their results show that for small drops (with $B \ll 1$) the speed decreases with increasing radius and that for $B \gg 1$ the drop velocity U eventually reaches a constant value close to $(4\sin\alpha)/3\lambda$, consistent with moving through parameter space from region FII (where $U \sim \alpha/(B^{1/2}\lambda)$) to region PII_1 (where $U \sim 4\alpha/3\lambda$, as in table 4). There is a difficulty here, however. Glycerol has viscosity 53 000 times that of air, so in this experiment $\lambda \gg \alpha^{-2}$, and our scaling argument suggests that a non-wetting drop should slide (rather than roll) with speed independent of Bond number. In the experiment, the drop rolls because wetting effects are present, the internal drop viscosity continues to drive the dynamics, and the upper boundary on region PII_1 in figure 12 does not apply.

Experiments reported in Aussillous & Quéré (2001) and Aussillous (2002), using high-viscosity droplets coated with hydrophobic powder, also demonstrated a transition between FII and PII_1-type behaviour. They measured $U \approx 3\alpha/2\lambda$ for $B > 1$ (although most of the data lie slightly beneath this estimate). The predicted coefficient $4/3$ for region PII_1 (table 4) agrees well with the measured data. Again, while we would expect air to lubricate a non-wetting drop with the viscosity ratios used experimentally, wetting effects mediated by the rough coating of the drop evidently extend the range of parameter space in which the PII_1 scalings apply. Roughness effects may explain why, when the experiments were repeated with lower-viscosity drops (Aussillous 2002), the dependence $U \propto 1/\lambda$ was not observed. Preliminary estimates suggest that for these parameter values the size of the roughness generated by the particles coating the drop becomes comparable with the thickness of the film. If roughness elements 'hold open' the layer beneath the drop, dissipation in this layer

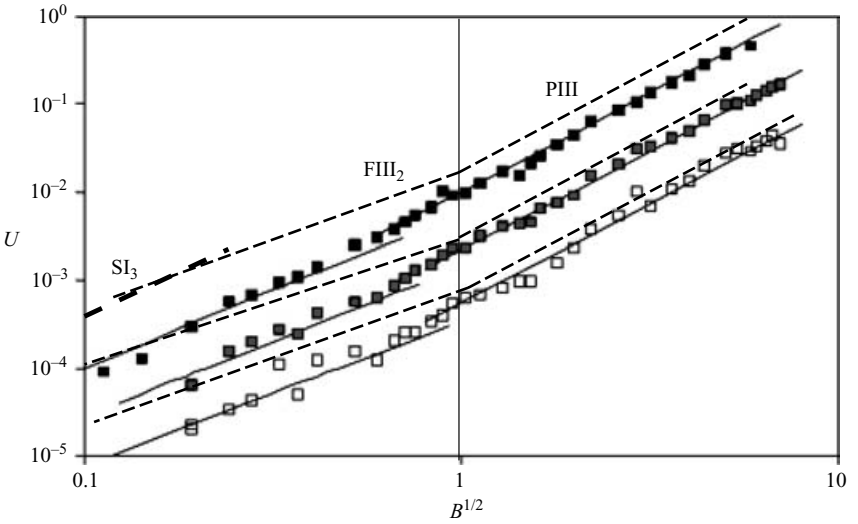

FIGURE 13. Speed of a bubble rising under an inclined plate as a function of scaled bubble radius $B^{1/2}$; data reproduced from Aussillous & Quéré (2002). Open, grey and black squares correspond to $\alpha = 0.012$, 0.035 and 0.22 respectively. The thin solid lines are straight-line fits of experimental data provided by Aussillous & Quéré, with the vertical intercept as an adjustable parameter. The dashed lines show the predictions given in table 4 for all three values of α for PIII and $FIII_2$, and for $\alpha = 0.22$ for SI_3.

may dominate that within the pancake, giving a further class of scaling behaviour dependent on the roughness length not explored in this paper.

Aussillous & Quéré (2002) also performed experiments to measure the speed at which an air bubble surrounded by a viscous fluid moves up a slightly inclined wall. They provide experimental data corresponding to regions SI_3, $FIII_2$ and PIII (figure 13). Predictions for each of these regions from table 4 are also shown in the figure. Predictions for region PIII show excellent agreement, particularly for smaller values of α. (Aussillous & Quéré independently derived the scaling relationship $U \sim (B^{3/4}\alpha)^{3/2}$.) The prediction for region $FIII_2$ for the smallest value of α is reasonable, but it worsens as α increases and B decreases. For $\alpha = 0.22$, the largest value used in the figure, $FIII_2$ spans only a small range of B ($\alpha \ll B^{1/2} \ll 1$). For $B^{1/2} \ll \alpha$ we enter region SI_3: here the prediction in table 4 has only logarithmic accuracy. The data do not support convincingly our prediction that the speed–radius curve should exhibit a clear change of slope across $B^{1/2} \sim \alpha$, although they are not inconsistent with this idea. The evident overlap between the regions SI_3 and $FIII_2$ justifies, at least for larger values of α, the use by Aussillous & Quéré (2002) of a composite approximation (the solid lines fitting the data points) combining a Stokes drag contribution (region SI_3) with a term of the form $(B\alpha^2)^{3/4}$.

8.2. *Conclusions*

We have used asymptotic methods to predict the behaviour of non-wetting drops sedimenting down a gently inclined plane. Restricting attention to low-capillary-number motion (with $B \ll \alpha^{-4/3}$ in three dimensions), for which surface tension ensures that the drop has a near-static shape everywhere except in the neighbourhood of the wall, we have shown that a three-dimensional drop exhibits

eleven asymptotically distinct types of motion (mapped out in figure 12 and table 3). As the Bond number B increases, the drop changes from being nearly spherical (S), to having a small but distinct flat spot at its base (F), to being pancake shaped (P). As the viscosity ratio λ increases, the drop's motion evolves from inviscid slipping, through rolling (or, for a pancake, tank-treading) to near-solid sliding. The scaling for the drop's speed may be determined by a balance between viscous dissipation in the lubricating film beneath the drop (I), the drop interior (II) or thin transition regions at either end of the film (III). The normal force supporting the drop on the wall is either static capillary pressure (regions F and P) or dynamic viscous pressure variations (region S). Detailed calculations using a force or couple balance as appropriate provide explicit leading-order predictions, summarized in table 4, for ten of the eleven regions in figure 12 (we have omitted detailed treatment of FII, which awaits a half-plane three-dimensional boundary-integral calculation), along with many of the borders between these regions. In two dimensions, a twelfth asymptotic region (CI_3) arises because of a peculiarity of two-dimensional flow, namely that a cylinder translating near a wall experiences zero net torque (Jeffrey & Onishi 1981).

Scalings for regions FII and PII_1 were predicted previously by Mahadevan & Pomeau (1999), and discussed further by Richard & Quéré (1999) and Aussillous & Quéré (2001). Scalings for regions PIII and $FIII_2$ were identified by Aussillous & Quéré (2002). To the best of our knowledge, the remaining predictions are new, as are the coefficients. These were determined by combining a capillary-statics approximation for the drop with lubrication theory for the thin lubricating film. For pancake-shaped drops, lubrication theory was used to describe the flow in the drop interior away from its ends. Coupling of the flow in the film to the flow in the drop is, in some cases, confined to the transition regions at either end of the film and to adjacent regions (with $O(1)$ aspect ratio) within the drop. As λ increases through a value $\tilde{\lambda}$ (shown with a dashed line on figure 12, the interface in these transition regions changes from being stress-free (with the drop in slipping motion) to having prescribed tangential velocity (with the drop in rolling or tank-treading motion). This fundamental change in drop kinematics affects the coefficients rather than the exponents in scaling relations. This change has been characterized by coupling a two-dimensional half-plane boundary-integral method to lubrication theory (Hodges *et al.* 2004).

While our results are not exact, they are asymptotically rational and should help provide support to future computational studies of this problem, as well as physical insight into the motion of viscous drops near boundaries.

An important extension of this study will be to treat transient motion, for example to understand better the 'bouncing' motion seen by DeBisschop *et al.* (2002) in their simulations of two-dimensional drops, to see how long it takes in an initial value problem for the predicted sliding solutions of very viscous drops to be realized, and to understand the relation between nearly uniform quasi-steady lubricating films formed beneath large drops on gently tilted slopes ($0 \ll \alpha \ll 1$) and unsteady dimples formed beneath drops on a horizontal plane ($\alpha = 0$, Yiantsios & Davis 1990). The case FII deserves particular attention because of its relevance to cell adhesion (Hodges & Jensen 2002), where viscous dissipation in a cell's interior is likely to influence strongly its rolling motion under shear flow on an adhesive surface.

Whilst some of the available data lend support to our estimates for drop speed and film thickness, it is clear that more experimental evidence directly related to this particular problem is required. It is often found (e.g. Cavanagh & Eckmann 1999; Richard & Quéré 1999; Kim, Lee & Kang 2002; Aussillous 2002) that a difficultly in observing drops moving down (or bubbles moving up) gently inclined walls stems

from the fact that small drops remain 'stuck' to the wall because of contact angle hysteresis. Only when the wall is tilted past some (relatively large) critical angle will the drop move. However, this is because most experiments focus on viscous partially wetting drops moving in air (or air bubbles suspended in liquid). More relevant to the present study would be to observe a viscous drop moving through another viscous liquid that strongly wets the wall, ensuring that the drop slides over a film and moves at very small inclination angles. We hope that the existence of this theoretical framework will stimulate new experiments in this area.

During the course of this work, S. R. H. was supported by an EPSRC research studentship. We are grateful for insightful comments from John Lister and L. Mahadevan.

REFERENCES

Abkarian, M., Lartigue, C. & Viallat, A. 2001 Motion of phospholipid vesicles along an inclined plane: Sliding and rolling. *Phys. Rev.* E **63**, 041906.

Aussillous, P. 2002 Doctoral thesis, Université Paris VI. Les gouttes enrobées.

Aussillous, P. & Quéré, D. 2001 Liquid marbles. *Nature* **411**, 924–927.

Aussillous, P. & Quéré, D. 2002 Bubbles creeping in a viscous liquid along a slightly inclined plane. *Europhys. Lett.* **59**, 370–376.

Bretherton, F. P. 1961 The motion of long bubbles in tubes. *J. Fluid Mech.* **10**, 166–188.

Burgess, D. & Foster, M. R. 1990 Analysis of the boundary-conditions for a Hele–Shaw bubble. *Phys. Fluids* A **2**, 1105–1117.

Cavanagh, D. P. & Eckmann, D. M. 1999 Interfacial dynamics of stationary gas bubbles in flows in inclined tubes. *J. Fluid Mech.* **398**, 225–244.

Davis, R. H., Schonberg, J. A. & Rallison, J. M. 1989 The lubrication force between two viscous drops. *Phys. Fluids* A **1**, 93–106.

DeBisschop, K. M., Miksis, M. J. & Eckmann, D. M. 2002 Bubble rising in an inclined channel. *Phys. Fluids* **14**, 93–106.

Goldman, A. J., Cox, R. G. & Brenner, H. 1967 Slow viscous motion of a sphere parallel to a plane wall. I. Motion through a quiescent fluid. *Chem. Engng Sci.* **22**, 637–651.

Hammond, P. S. 1982 PhD Thesis, University of Cambridge.

Hodges, S. R. 2002 PhD Thesis, University of Cambridge.

Hodges, S. R. & Jensen, O. E. 2002 Spreading and peeling dynamics in a model of cell adhesion. *J. Fluid Mech.* **460**, 381–409.

Hodges, S. R., Jensen, O. E. & Rallison, J. M. 2004 The motion of a viscous drop through a cylindrical tube. *J. Fluid Mech.* **501**, 279–301.

Jeffrey, D. J. & Onishi, Y. 1981 The slow motion of a cylinder next to a plane wall. *Q. J. Mech. Appl. Maths* **34**, 129–137.

Jensen, O. E. 2000 Draining collars and lenses in liquid-lined vertical tubes. *J. Colloid Interface Sci.* **221**, 38–49.

Kim, H. Y., Lee, H. J. & Kang, B. H. 2002 Sliding of liquid drops down an inclined solid surface *J. Colloid Interface Sci.* **247**, 372–380.

Landau, L. D. & Levich, B. 1942 Dragging of a liquid by a moving plate. *Acta Physicochim. URSS* **17**, 42–54.

Magnaudet, J., Takagi, S. & Legendre, D. 2003 Drag, deformation and lateral migration of a buoyant drop moving near a wall. *J. Fluid Mech.* **476**, 115–157.

Mahadevan, L. & Pomeau, Y. 1999 Rolling droplets. *Phys. Fluids* **11**, 2449–2453.

Masliyah, J., Jauhari, R. & Gray, M. 1994 Drag coefficients for air bubbles rising along an inclined surface. *Chem. Engng Sci.* **49**, 1905–1911.

Neitzel, G. P. & Dell'Aversana, P. 2002 Noncoalescence and nonwetting behavior of liquids. *Annu. Rev. Fluid Mech.* **34**, 267–289.

O'Brien, S. B. G. 1991 On the shape of small sessile and pendant drops by singular perturbation techniques. *J. Fluid Mech.* **233**, 519–537.

O'Neill, M. E. & Stewartson, K. 1967 On the slow motion of a sphere parallel to a nearby plane wall. *J. Fluid Mech.* **27**, 705–724.

Richard, D. & Quéré, D. 1999 Viscous drops rolling on a tilted non-wettable solid. *Europhys. Lett.* **48**, 286–291.

Rienstra, S. W. 1990 The shape of a sessile drop for small and large surface tension. *J. Engng Maths* **24**, 193–202.

Tsao, H.-K. & Koch, D. L. 1997 Observations of high Reynolds number bubbles interacting with a rigid wall. *Phys. Fluids* **9**, 44–56.

Wong, H., Radke, C. J. & Morris, S. 1995 The motion of long bubbles in polygonal capillaries. Part 1. Thin films. *J. Fluid Mech.* **292** 71–94.

Yiantsios, S. G. & Davis, R. H. 1990 On the buoyancy-driven motion of a drop towards a rigid surface or a deformable interface. *J. Fluid Mech.* **217**, 547–573.